Supplemental Appendix

Cardiac Spinal Afferent Denervation Attenuates Renal Dysfunction in Rats With Cardiorenal Syndrome Type 2*

Zhiqiu Xia, MD, PhD,[a] Neetha Nanoth Vellichirammal, PhD,[b] Li Han, PhD,[a,c] Lie Gao, MD, PhD,[d] Erika I. Boesen, PhD,[d] Alicia M. Schiller, PhD,[a] Peter Pellegrino, MD, PhD,[a] Steven J. Lisco, MD,[a] Chittibabu Guda, PhD,[b,e] Irving H. Zucker, PhD,[d] Han-Jun Wang, MD[a,d]

From the [a]Department of Anesthesiology, University of Nebraska Medical Center, Omaha, Nebraska, USA; [b]Department of Genetics, Cell Biology, and Anatomy, University of Nebraska Medical Center, Omaha, Nebraska, USA; [c]College of Veterinary Medicine, Huazhong Agricultural University, Wuhan, China; [d]Department of Cellular and Integrative Physiology, University of Nebraska Medical Center, Omaha, Nebraska, USA; and [e]Bioinformatics and Systems Biology Core, University of Nebraska Medical Center, Omaha, Nebraska, USA.

Supplemental Methods

All animal experimentation was approved by the Institutional Animal Care and Use Committee of the University of Nebraska Medical Center and performed in accordance with the National Institutes of Health's *Guide for the Care and Use of Laboratory Animals*. Experiments were performed on adult, male, 400–500-g Sprague-Dawley rats purchased from the Charles River Laboratories. Animals were housed on-site and given a one-week acclimation period prior to

experimentation. Food and water were supplied *ad libitum*, and rats were housed on a 12-hour light/dark cycle. The overall experimental protocol is outlined in Supplemental Figure 1.

Rat model of CHF and chronic cardiac sympathetic afferent desensitization

Myocardial infarction (MI)–induced CHF was produced by coronary ligation as previously described.[1] Briefly, rats were anesthetized with 2%-3% isoflurane-oxygen mixture during the surgical procedure with positive pressure mechanical ventilation at a rate of 60 breaths per min. A left thoracotomy was performed through the fifth intercostal space to expose the heart and the pericardium was opened. The left anterior descending coronary artery was ligated with a 6-0 silk suture. The thorax was closed and intrapleural pressure was re-established. Sham animals underwent the same procedure, including the thoracotomy, except no coronary ligation was performed. Buprenorphine (0.05 mg/kg, SC) was given once immediately following surgery and on post-operative day 1 and 2 for alleviation of pain. Cardiac function including ejection fraction (EF) and fractional shortening (FS) were measured using high frequency echocardiography (VEVO 3100; Visual Sonics). At the time of terminal experiments, rat infarct size was determined as previously described.[1] Rats (n=16) with less than 15% infarct size were considered as mild infarction and excluded from this study.

In a subgroup of the rats that were assigned to receive MI procedures, the epicardial application of resiniferatoxin (RTX; 50 μg/mL) was performed to desensitize the CSAR by afferent ablation as previously described.[1] RTX (Sigma-Aldrich; 50 μg/mL) was painted twice on the entire surface of the left and right ventricles with a small brush just prior to coronary artery ligation. Vehicle (2 mL of ethanol mixed with 18 mL of Tween in isotonic saline) was painted on the ventricles as a control. The dose of RTX was determined in a previous study[1] in which we found

nearly complete ablation of TRPV1-expressing cardiac nerve endings on the surface of the rat heart. The same dose of RTX also abolished functional activation of the CSAR by epicardial application of exogenous bradykinin (BK; 10 μg/mL).[1]

Hemodynamic, renal blood flow measurements, and activation of the CSAR

In acute terminal experiments, rats were anesthetized with urethane (800 mg/kg I.P) and α-chloralose (40 mg/kg IP). The trachea was cannulated, and the rat was ventilated artificially with room air supplemented with 100% oxygen. A heating pad was used to maintain body temperature at approximately 37 °C during the experiment. Left ventricular end-diastolic pressure (LVEDP) and left ventricular end-systolic pressure (LVESP) were measured using a Millar catheter (SPR 524; size, 3.5 F; Millar Instruments) that was placed though the right carotid artery into the left ventricle. Arterial pressure (AP) and mean arterial pressure (MAP) were recorded when the Millar catheter was pulled back into the aorta. Heart rate (HR) and MAP were derived from the AP pulse using LabChart 7.1 software and a PowerLab model 16S (ADInstruments) data acquisition system. A polyethylene catheter was placed in the right jugular vein for intravenous injections. After jugular vein cannulation, the cervical vagi were sectioned bilaterally in order to isolate the CSAR from vagally mediated reflexes. A perivascular flow probe (0.5 VB587; Transonic Systems), connected to a flow meter (T106 small animal flow meter; Transonic Systems), was placed around the left renal artery to allow continuous recording of renal blood flow (RBF) both at rest and during CSAR activation. Renal vascular resistance (RVR) was calculated as MAP/RBF. To activate the CSAR, a left thoracotomy was performed through the fourth intercostal space, and the heart was exposed. A square of filter paper (3 mm × 3 mm) saturated with BK (10 μg/mL) was applied to the anterior surface of the left ventricle to

activate regional cardiac spinal afferents in vagotomized rats. Hemodynamic changes were continuously recorded before and after the BK application. At the end of the experiment, the rat was euthanized with an overdose of saturated potassium chloride.

CVP measurements

The central venous pressure (CVP) was measured in the conscious state utilizing the radiotelemetry technique. Under 2% isoflurane anesthesia, the rat was placed in the supine position. After making a 10–15-mm incision in the frontal neck area, the right external jugular vein was identified and dissected. The catheter of a telemetry unit (PA-C10; Data Science International) was inserted into the jugular vein and further advanced into the caudal vena cava to the right atrium level. The telemetry unit was then secured to connective tissue with a 4-0 suture and buried under the skin in mid-scapula area. Three days after surgery, the CVP was continuously recorded for 24 hours at a sampling rate of 1 kHz using a PowerLab data acquisition system with LabChart 7 software (model 8S; ADInstruments). The final CVP was obtained by averaging 24-hour values.

Renal function

A blood sample of ~100 μL was obtained from the rat tail veins at various time points after MI or sham surgery. These were 6-8, 12-14, and 16-18 weeks. Renal function was evaluated by measuring potassium, creatinine, and blood urea nitrogen (BUN) with the use of iSTAT analysis (Abbott).

GFR measurement

Glomerular filtration rate (GFR) was measured using clearance of fluorescein isothiocyanate (FITC)–inulin (Sigma) at 16-18 weeks post-MI. Rats were anesthetized with urethane (800 mg/kg IP) and α-chloralose (40 mg/kg IP) and then ventilated with room air supplemented with 100% oxygen. A heating table was used to maintain body temperature at 37°C throughout the experiment. A catheter was placed though the right carotid artery into the left ventricle for blood sample collection. A polyethylene catheter was placed in the right jugular vein for intravenous administration of FITC-inulin. A bolus dose of 8 mg/mL FITC-inulin was initially administered followed by constant infusion of 4 mg/mL at 50 μL/min. A catheter was placed into the bladder via a suprapubic incision and urine was collected continuously. The FITC-inulin concentration in urine and plasma were measured using a fluorescence microplate reader at 480 nm excitation and 520 nm emission. The formula below was used for calculation of GFR.

$$\text{GFR} = \frac{\text{Urine flow rate} \times \text{Urine inulin concentration}}{\text{Plasma inulin concentration}}$$

Urinary Kim-1 and albuminuria

Twenty-four-hour urine was collected in metabolic cages, followed by centrifugation to remove any particulates and then stored at −80 °C. Urinary osmolality was measured with a Vapro Pressure Osmometer (D.A.I. Scientific Equipment). Urinary kidney injury molecule 1 (Kim-1) levels were measured by using Rat TIM-1/KIM-1/HAVCR Immunoassay (R&D Systems) according to the manufacturer's instructions. Urinary albumin concentration was measured by the Physiology Core Laboratory at the Medical College of Wisconsin.

Histologic evaluation

The kidneys from Sham, CHF+vehicle, and CHF+RTX rats at ~4 months post-MI were fixed in 4% paraformaldehyde solution, embedded in paraffin, cut into 5-μm serial sections, and stained with Masson trichrome or periodic acid–Schiff (PAS) staining by the tissue core facility at the University of Nebraska Medical Center. In order to evaluate tubular injury, 10 high-powered (×20) fields (5 cortical fields and 5 medullary fields) of PAS-stained kidney sections were randomly selected per rat, and the percentage area of tubules that were classified as normal, dilated, containing casts, or necrotic was calculated by overlaying a 10 × 10 grid of points on each image, similar to the method described in the previous study.[2] The Masson trichrome-positive area or PAS-positive area relative to the whole area (10 cortical fields and 10 medullary fields per rat) was analyzed using Image J software (National Institutes of Health). In addition, Masson trichrome stained sections were scored semiquantitatively using the following scale: score 0: no fibrosis; score 1: <25% fibrotic tubules; score 2: 25%-50% fibrotic tubules; score 3: 50%-75% fibrotic tubules; score 4: >75% fibrotic tubules.

RNA isolation, sequencing, and read alignment

The Qiagen miRNeasy kit was used to isolate total RNA from homogenized kidney tissue from sham, CHF+vehicle, and CHF+RTX rats according to the manufacturer's instructions. RNAseq libraries were prepared from 500 ng total RNA for each sample using the NEBNext Ultra RNA Library Prep Kit for Illumina with the NEBNext Poly(A) mRNA Magnetic Isolation Module following the manufacturer's recommended protocol.

Trimming low-quality ends from reads, and adapter trimming was performed using cutadapt.[3] Reads were mapped against the genome reference mm10 using STAR aligner v2.3.0.[4] Aligned reads were further filtered to exclude transcripts for which the maximum number of reads for all samples was >40 reads to eliminate noise and genes with low read counts. Raw sequencing data were submitted to the NCBI sequence read archive (SRA accession: SRR17497176, SRR17497171, SRR17497169, SRR17497175, SRR17497174, SRR17497173, SRR17497172, SRR17497170, SRR17497168, SRR17497167; BioProject: PRJNA795520).

Differential expression analyses and pathway enrichment analyses

The read count data were exported to DESeq2v1.18.1[5] to identify differentially expressed genes using the negative binomial distribution from normalized read count data. Pairwise comparisons were made between sham and CHF+vehicle, sham and CHF+RTX, and CHF+vehicle and CHF+RTX. A gene was considered significantly differentially expressed if its corresponding Benjamin-Hochberg false discovery rate (FDR) corrected *P* value[6] was ≤0.05, and if it had an absolute log2 fold change ≥1.5. Gene annotation enrichment analysis of differentially regulated proteins to identify known functions, pathways, and networks effected was performed using Ingenuity Pathway Analysis (IPA; Ingenuity Systems). The significance was set at a *P* value of 0.05. Network representations of enriched pathways and Gene Ontology (GO) terms associated with the biological process were graphically represented using ClueGO cytoscape plug-in.[7] Clustered heat map of differentially expressed genes was plotted using the heatmap.2 function of the R package gplots (https://cran.r-project.org/web/packages/gplots/).[8]

Validation of RNA sequencing data with real-time quantitative PCR

Kidney tissues were harvested and dissected into cortex and medulla at different time points (1 week, 4 weeks, 8 weeks, and 18 weeks post-MI), and then small pieces of the kidney cortex and medulla from sham, CHF+vehicle, and CHF+RTX were frozen at −80 °C, from which RNA was purified by using the RNeasy Mini RNA purification kit (Qiagen). cDNA was generated from RNA using the QuantiTect Reverse Transcription Kit (Qiagen), according to the manufacturer's instructions. For the measurements of the mRNA expression of *Kim-1*, neutrophil gelatinase–associated lipocalin (*Ngal*), interleukin-1beta (*Il1b*), interleukin-6 (*Il6*), and other genes, real-time quantitative polymerase chain reaction (RT-PCR) was performed by using the QuantiFast SYBR Green PCR Kit (Qiagen). Primer sequences for RT-PCR are listed in Supplemental Table 1. Reaction conditions were set according to the manufacturer's instructions. The Ct (threshold cycle) values of the target gene amplifications were normalized to those of the actin-beta (*Actb*). Each biological replicate was measured with three technical replicates, and fold change was calculated using the $2^{-\Delta\Delta Ct}$ method. Primers were designed and synthesized by Integrated DNA Technologies based on published sequences (http://www.ncbi.nlm.nih.gov).

Survival analysis

Survival was monitored from 1 week post-MI through study end point (up to 6 months). The condition of each rat was monitored and recorded every day. Acute death occurring within 1 week after MI was not included in the survival analysis.

Intrastellate injection of RTX

Experiments were performed on adult, male, 400–500-g Sprague-Dawley rats purchased from the Charles River Laboratories. MI-induced CHF was produced by coronary ligation as

previously described.[1] Four weeks after MI, these rats were randomized to either bilateral intra-stellate injection of RTX (CHF+SG RTX group) or sham surgery group (CHF+SG Veh group). Intra-stellate injection of RTX was done as previously described.[9] Briefly, rats were mechanically ventilated with 3% isoflurane-oxygen mixture. The internal thoracic and costocervical arteries were exposed medially to the origins of where the stellate ganglia are located. RTX (5 μL, 50 mg/mL) was injected into the left and right stellate ganglia over 30s. To validate the SG injection of RTX, rats were anesthetized with urethane (800 mg/kg IP) and α-chloralose (40 mg/kg IP). AP and HR were measured as described above. RSNA was recorded as previously described.[10] Epicardial application of BK was used to activate cardiac spinal afferents as described by us previously.[11] In brief, the chest was opened through the fourth intercostal space. To activate cardiac spinal afferents, a square of filter paper (3 × 3 mm) saturated with BK (10 μg/mL; Sigma Aldrich) was applied randomly to the surface of the left ventricular free wall. Hemodynamics and RSNA were continuously recorded. After the responses peaked, the heart was rinsed 3 times with 10 mL warm normal saline solution.

Renal denervation

Experiments were performed on adult male 400–500-g Sprague-Dawley rats purchased from the Charles River Laboratories. MI-induced CHF was produced by coronary ligation as previously described.[1] Four weeks after the MI procedure, rats were randomized to either the URDN group or the sham surgery group. Under anesthesia with 3% isoflurane, the left renal arteries and veins were exposed by a left flank incision. All visible left renal nerve bundles were cut followed by painting the left renal artery with 10% phenol in alcohol. The sham-operated rats received similar procedures with the exception that the renal nerves remained intact. Renal

norepinephrine (NE), dopamine (DOPA), epinephrine (Epi), and serotonin were quantified with the assistance of Dr. Gregory Fink in the Department of Pharmacology and Toxicology at the Michigan State University. At different time points, prior to URDN, 8 weeks post-MI and 16 weeks post-MI, echocardiography was performed to evaluate cardiac function. GFR was measured at 16-18 weeks post-MI. Renal tissues from the left and right kidneys were harvested and dissected into cortex and medulla. The mRNA expression of *Kim-1*, *Ngal*, *Il1b*, and *Il6* were measured using the QuantiFast SYBR Green PCR Kit (Qiagen).

Statistics

All data are expressed as the mean ± SD and were analyzed using GraphPad Prism 9.0 (GraphPad Software. Shapiro-Wilk test was used for assessing distribution. The 2-tailed Student *t* test and 1-way analysis of variance (ANOVA) were used for data that were normally distributed, and the Mann-Whitney *U* test and Kruskal-Wallis test were used for data that were not normally distributed. Differences between groups were determined by a 2-way ANOVA followed by Tukey's post hoc test for multiple pairwise comparisons. Survival estimates between vehicle-treated and RTX-treated rats, conditional on survival until end of week 1 post-MI, were calculated using Kaplan-Meier methods and compared using the log-rank test. $P < 0.05$ was considered to be statistically significant.

Supplemental Results

RNA sequencing analysis in kidney tissues of rats with CHF treated with epicardial vehicle or RTX

To further investigate the pathophysiological mechanisms of CRS type 2, RNA sequencing of the whole kidneys was performed in sham, CHF+vehicle, and CHF+RTX rats. Sequencing of these transcriptomes yielded more than 100 million 75-mer single-end high-quality reads from a total of 11 samples (5 replicates for sham, and three replicates each for CHF+vehicle and CHF+RTX). The average number of raw reads per sample was 21 million. The average mapping percentage of the raw reads to the reference transcripts was 50%.

Of the 394 genes differentially expressed between sham and CHF+vehicle rats, the majority (n = 359) were up-regulated in CHF+vehicle (**Table S4; Supplemental Figure 2**). The RNA sequencing shows that gene expression of *Kim-1* (*Havcr1*) was increased by ~104-fold and *Ngal* (*Lcn2*) was increased by ~36-fold in whole-kidney tissues of CHF+vehicle rats compared with sham rats. In addition, RNA sequencing demonstrated that gene expression of the proinflammatory cytokine, *Il6* was significantly up-regulated by ~40-fold at 18 weeks post-MI. Expression of genes related to cell death and survival, such as *Il24* and nephroblastoma overexpressed (*Nov*) were increased by ~55-fold and ~4-fold, respectively. Interestingly, 2 hypoxia-related genes, receptor-type tyrosine-protein phosphatase zeta (*Ptprz1*) and hypoxia-inducible factor 3 alpha (*Hif3a*), were also up-regulated by ~6- and ~7-fold, respectively.

Significantly enriched GO categories for differentially expressed genes between sham and CHF+vehicle groups are shown in **Table 2** and **Supplemental Figure 3**. The MAPK signaling pathway, the pathway related to cytokine–cytokine receptor interaction, and tumor necrosis factor (Tnf) signaling pathway were up-regulated in the kidneys of CHF+vehicle rats. In addition, Hif-1 signaling and apoptosis-related pathways were activated in CHF+vehicle rats compared

with sham. IPA analysis (**Supplemental Table 5**) identified the Il-6 signaling pathway to be enriched (P = 4.48E−09; overlap = 12.1%).

Comparison of the gene expression profile of CHF+vehicle and CHF+RTX rats revealed an entirely different profile, with the majority of the differentially expressed genes down-regulated in CHF+RTX rats (**Supplemental Table 6**). A total of 124 genes were differentially expressed between CHF+vehicle and CHF+RTX rats, and 96 genes were down-regulated in CHF+RTX (**Supplemental Figure 4**). *KIM-1* (*Havcr1*) expression was only increased by ~5-fold in CHF rats treated with RTX compared with sham rats (**Figure 3C**). However, *Ngal* was similarly elevated in both CHF+vehicle and CHF+RTX rats. Gene expression for *Il24*, *Nov*, and *Ptprzl1* were reduced compared with that in CHF+vehicle rats. Enriched GO categories showed that pathways that regulate the Il-1β secretion were enhanced after RTX treatment (**Supplemental Figure 5**). Surprisingly, pathways that can negatively regulate blood vessel diameter were also enhanced, implying that RTX may improve renal perfusion through ameliorating intra-renal vasoconstriction. IPA analysis identified several pathways that are involved in Il-12 signaling and production in macrophages, LXR/RXR activation, and Wnt/β-catenin signaling were enriched (**Supplemental Table 7**).

Subsequently, we analyzed genes that were common between the two comparisons, (ie, sham vs CHF+vehicle, and CHF+vehicle vs CHF+RTX). We found 23 genes that were common among these comparisons (**Figure 3**). The majority of these 23 genes showed a reversal in gene expression in CHF+RTX rats. For example, *Kim-1* (*Havcr1*) was up-regulated in CHF+vehicle rats compared with sham, but down-regulated in CHF-RTX rats compared with CHF+vehicle rats (**Table 2**). Cellular death–associated genes, such as *Il24* and *Nov*, showed the same trend. Interestingly, *Ptprz1*, which has been found to be expressed in human embryonic kidney cells

under hypoxic conditions, was up-regulated in CHF+vehicle rats was also attenuated by RTX. In addition, α-1d adrenergic receptor (*Adra1d*) was up-regulated in CHF+vehicle rats and was attenuated by RTX.

Pathways affected during the development of CRS type 2 with and without CSAR ablation

Among the differentially expressed genes between sham and CHF+vehicle rats, the apoptotic pathway was the most affected. Of the 96 differentially expressed genes associated with apoptosis, the majority were up-regulated in CHF+vehicle rats compared with sham rats (**Supplemental Figure 6**). Eleven genes were differentially regulated in the hypoxia pathway. All of the genes associated with hypoxia were up-regulated in CHF+vehicle rats (**Supplemental Figure 7**). Differentially expressed genes associated with inflammation also followed the same trend, with the majority up-regulated in CHF+vehicle rats (**Supplemental Figure 8**). All of the differentially expressed genes between sham and CHF+vehicle rats that are associated with kidney damage were up-regulated in CHF+vehicle rats (**Supplemental Figure 9**). Interestingly, the majority of the differentially expressed genes associated with apoptosis were down-regulated in CHF+RTX rats (**Supplemental Figure 10**). This trend was also noted for genes associated with inflammation (**Supplemental Figure 11**) and kidney damage (**Supplemental Figure 12**).

To validate the effects of RTX on mRNA expression of *Kim-1*, subsequent RT-PCR experiments were performed. In the renal cortex of CHF+vehicle rats *Kim-1* mRNA level was increased by ~300-fold, which was largely prevented in CHF+RTX rats (only 4-fold increase). A similar trend was observed in the renal medulla. However, the mRNA expression of *Ngal* were comparable in the renal cortex and medulla of CHF+vehicle rats and CHF+RTX rats compared with sham rats (**Figures 4A-4D**). mRNA expressions of *Il6* in the renal cortex and medulla were increased in

CHF rats regardless of treatment. However, mRNA expression of *Il1b* in the renal cortex was increased by ~4 fold in CHF+vehicle rats, which was attenuated by RTX treatment. In the renal medulla, RTX did not alter mRNA expression of *Il1b* in the CHF+vehicle rats (**Figures 4E-4H**).

Time-course changes of kidney damage markers after MI

To determine the time course of renal damage markers, mRNA expression of *Kim-1* and *Ngal* were measured in the renal cortex and medulla (**Figure 4 I-L**). We found that both *Kim-1* and *Ngal* levels were increased at 4 weeks post-MI, suggesting the occurrence of acute kidney injury in the early stages post-MI. Surprisingly, 8 weeks after MI, *Kim-1* and *Ngal* expression was undetectable. Eighteen weeks post-MI, *Kim-1* and *Ngal* expression increased again. Changes in blood chemistry that indicate renal dysfunction were detected around the same time window (16-18 weeks post-MI) in CHF+vehicle rats (**Table 1**). Therefore, in our rat model of CHF, we considered 16-18 weeks post-MI as the experimental window to study the CRS type 2.

RNA sequencing data suggest that several genes related to inflammation, apoptosis, and hypoxia were also involved in the development of renal dysfunction. Therefore, the time-course changes of the expression of those genes were also evaluated. Gene expression of inflammatory cytokines including *Il6*, *Il1b*, and inducible nitric oxide synthase (*iNos*) was increased during the early stage (1 week and/or 4 weeks) post-MI. The expression in rats with 8 weeks post-MI was comparable with that in sham rats, whereas the expression increased again at 4 months post-MI (**Supplemental Figures 13A-S13D, 13G, and 13H**). However, the expression of tumor necrosis factor alpha (*Tnfa*) only increased at 4 weeks post-MI (**Supplemental Figures 13E and 13F**).

Gene expression of *Hif1a* and *Hif3a* was increased at 1 month post-MI (**Supplemental Figures 14C-14F**). However, gene expression of erythropoietin (*Epo*), which is regulated by the Hif-1

signaling pathway and is also an indicator of severe renal failure, was increased at the late stage post-MI, consistent with the development of renal dysfunction at 4 months post-MI (**Supplemental Figures S14A and S14B**).

Activating transcription factor 3 (Atf3) is induced on physiologic stress in various tissues and is involved in the apoptotic process. Gene expression of *Atf3* was immediately increased after myocardial infarction (1 week post-MI) and at the late stage (4 months post-MI). Interestingly, gene expression of *Atf3* between 1 week and 8 weeks post-MI was normal (**Supplemental Figures 15A and 15B**).

Heme oxygenase 1 (HMOX1) participates in anti-inflammatory processes as well as apoptotic processes by up-regulating interleukin 10 (*Il10*) and interleukin 1 receptor antagonist (*Il1ra*) expression. Gene expression of *Hmox1* was increased at 4 weeks post-MI. Similarly, 8 weeks post-MI, the expression of *Hmox1* was comparable with that in sham rats. However, the expression increased again at 4 months post-MI (**Supplemental Figures 15C and 15D**). In addition, gene expression for arginine vasopressin receptor 2 (*Avpr2*) was decreased at 4 months post-MI in CHF+vehicle rats (**Supplemental Figures 15E and 15F**).

Intrastellate injection of RTX 4 weeks post-MI prevents renal dysfunction in rats with CHF

Local application of RTX into stellate ganglia effectively reduced the CSAR (**Supplemental Figure 16**). To evaluate the effects of the application of RTX to the stellate ganglia on cardiac remodeling in CHF rats, LV dimensions and volumes at different time points post-MI were performed. Intrastellate RTX injection tended to prevent the chamber dilation following MI while this change did not reach a statistic difference (**Supplemental Figure 17**).

Renal function was evaluated at 16 weeks post-MI. Blood analysis of creatinine, BUN, and electrocytes are summarized in **Table 3**. Compared with CHF+SG vehicle, SG injection of RTX reduced the BUN and tended to decrease plasma potassium, implying that SG injection of RTX improved renal function in the setting of CHF.

To further evaluate renal dysfunction developed during the progression of CHF, mRNA expression of *Kim1* and *Ngal* were measured. The mRNA level of *Kim1* in the renal cortex was significantly increased in the CHF+SG vehicle rats but not in the CHF+SG RTX rats compared with sham rats (**Figure 7A**). Similar trends were observed in the medulla (**Figure 7B**). on the other hand, the mRNA level of *Ngal* in both renal cortex and medulla was comparable between CHF+SG vehicle and CHF+SG RTX rats (**Figures 7C and 7D**). The mRNA expression of *Il1b* and *Il6* in the kidneys were examined to investigate the effects of SG injection of RTX on inflammation. Similarly, the mRNA expression of *Il6* tended to increase in the kidneys of CHF+SG vehicle and CHF+SG RTX rats. However, compared with sham rats, the changes of mRNA expressions of *Il1b* in the CHF+SG vehicle and CHF+SG RTX rats did not reach significance (**Figures 7E-7H**).

NE measurements in renal tissues of sham and CHF rats with and without renal denervation

There was no difference in NE levels between the sham-operated kidneys and the non-operated kidneys in CHF rats (**Supplemental Figure 18**). The renal NE levels of CHF rats were comparable with that in the sham group. Compared with the non-operated kidneys in the CHF+URDN group, a reduction in NE of 79.2% was found in denervated kidneys 12 weeks after URDN surgery, which was 16 weeks post-MI.

No significant difference in the levels of DOPA or epinephrine were detected among the left and right kidneys from the sham, CHF, and CHF+URDN groups (**Supplemental Figures 19A and 19B**). The dopamine levels in the sham-operated kidneys and non-operated kidneys were higher than that in the sham group. A decrease in the dopamine levels in the denervated kidneys was detected compared with that in the contralateral side (**Supplemental Figure 19C**). Interestingly, the serotonin level in the denervated kidneys was increased compared with those in the sham group, CHF group and the non-operated side in the CHF+URDN group (**Supplemental Figure 19D**).

References

1. Wang HJ, Wang W, Cornish KG, Rozanski GJ, Zucker IH. Cardiac sympathetic afferent denervation attenuates cardiac remodeling and improves cardiovascular dysfunction in rats with heart failure. *Hypertension*. 2014;64:745-755.
2. Boesen EI. ET(A) receptor activation contributes to T cell accumulation in the kidney following ischemia-reperfusion injury. *Physiol Rep*. 2018;6:e13865.
3. Martin M. Cutadapt removes adapter sequences from high-throughput sequencing reads. *EMBnet J*. 2011;27:10-12.
4. Dobin A, Davis CA, Schlesinger F, et al. STAR: ultrafast universal RNA-seq aligner. *Bioinformatics*. 2013;29:15-21.
5. Love MI, Huber W, Anders S. Moderated estimation of fold change and dispersion for RNA-seq data with DESeq2. *Genome Biol*. 2014;15:550.
6. Benjamini Y, Hochberg Y. Controlling the false discovery rate: a practical and powerful approach to multiple testing. *J R Stat Soc Ser B*. 1995;57:289-300.
7. Bindea G, Mlecnik B, Hackl H, et al. ClueGO: a Cytoscape plug-in to decipher functionally grouped gene ontology and pathway annotation networks. *Bioinformatics*. 2009;25:1091-1093.
8. Blighe K, Rana S, Lewis M. EnhancedVolcano: Publication-ready volcano plots with enhanced colouring and labeling. R package version 1.4.0, 2019. Available at: https://github.com/kevinblighe/EnhancedVolcano
9. Hahka TM, Xia Z, Hong J, et al. Resiniferatoxin (RTX) ameliorates acute respiratory distress syndrome (ARDS) in a rodent model of lung injury. *bioRxiv*. 2020:2020.09.14.296731.

10. Gao L, Schultz HD, Patel KP, Zucker IH, Wang W. Augmented input from cardiac sympathetic afferents inhibits baroreflex in rats with heart failure. *Hypertension*. 2005;45:1173-1181.

11. Shanks J, Xia Z, Lisco SJ, et al. Sympatho-excitatory response to pulmonary chemosensitive spinal afferent activation in anesthetized, vagotomized rats. *Physiol Rep*. 2018;6:e13742.

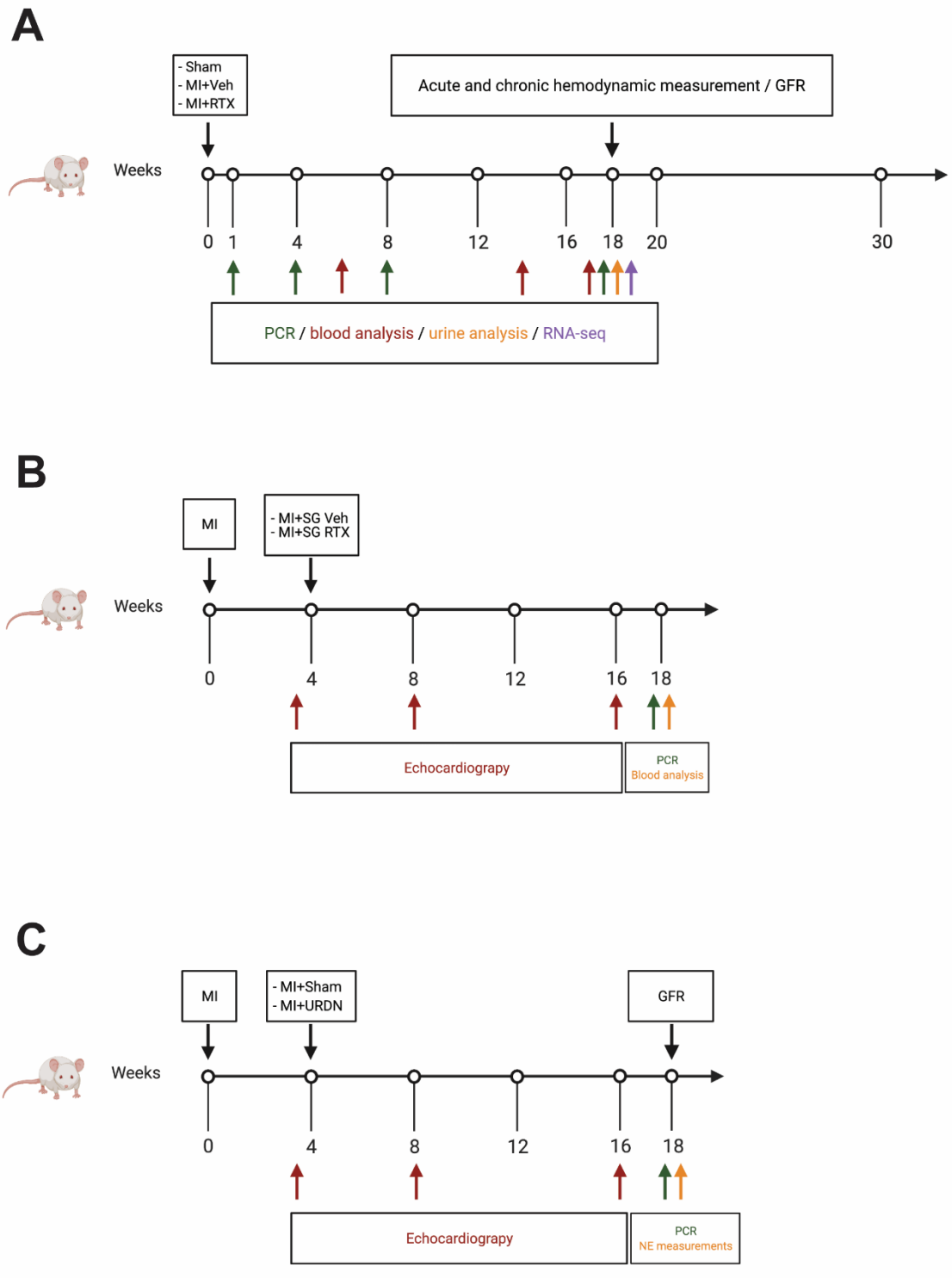
A
- Sham
- MI+Veh
- MI+RTX
Acute and chronic hemodynamic measurement / GFR
Weeks
0 1 4 8 12 16 18 20 30
PCR / blood analysis / urine analysis / RNA-seq
B
MI
- MI+SG Veh
- MI+SG RTX
Weeks
0 4 8 12 16 18
Echocardiograpy
PCR
Blood analysis
C
MI
- MI+Sham
- MI+URDN
GFR
Weeks
0 4 8 12 16 18
Echocardiograpy
PCR
NE measurements

Supplemental Figure 1. Schematic diagrams of study design. A, Epicardial application of RTX. B, Intra-stellate injection of RTX. C, Unilateral renal denervation (URDN). Figure made with BioRender.com.

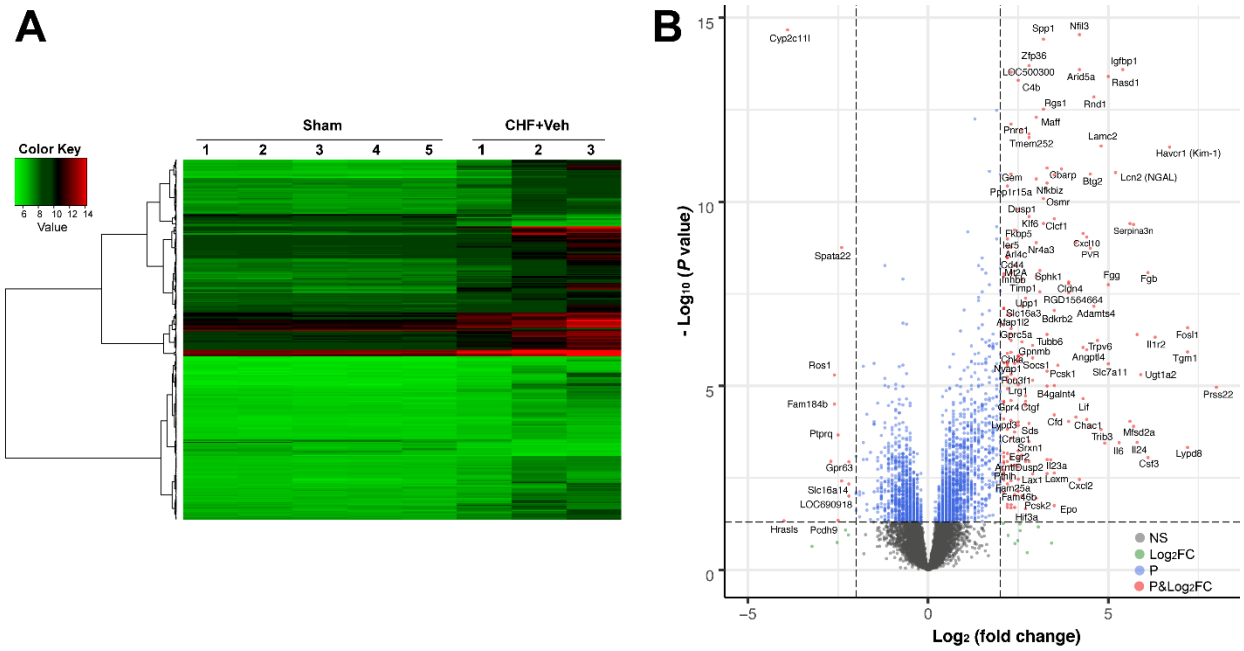

Supplemental Figure 2. A. Heat map of differentially expressed genes in kidneys from CHF+vehicle rats when compared with sham. Genes were clustered according to their expression profile. Red representing higher level of expression and blue representing lower expression. Gene expression values were converted to *z*-scores to facilitate comparison, and for visual clarity. B. A volcano plot of differentially expressed genes between CHF and sham. The red dots represent differentially expressed genes with at least 1 $\log_2$ fold-change between CHF compared with sham and Benjamini-Hochberg (BH) adjusted $P < 0.05$; green and blue dots indicate genes with $\log_2$ fold change ≥1 or BH adjusted $P \leq 0.05$ respectively. Gray dots indicate genes that did not meet the cutoff for fold change or *P* value. Sham group, n=5; CHF+Veh group, n=3.

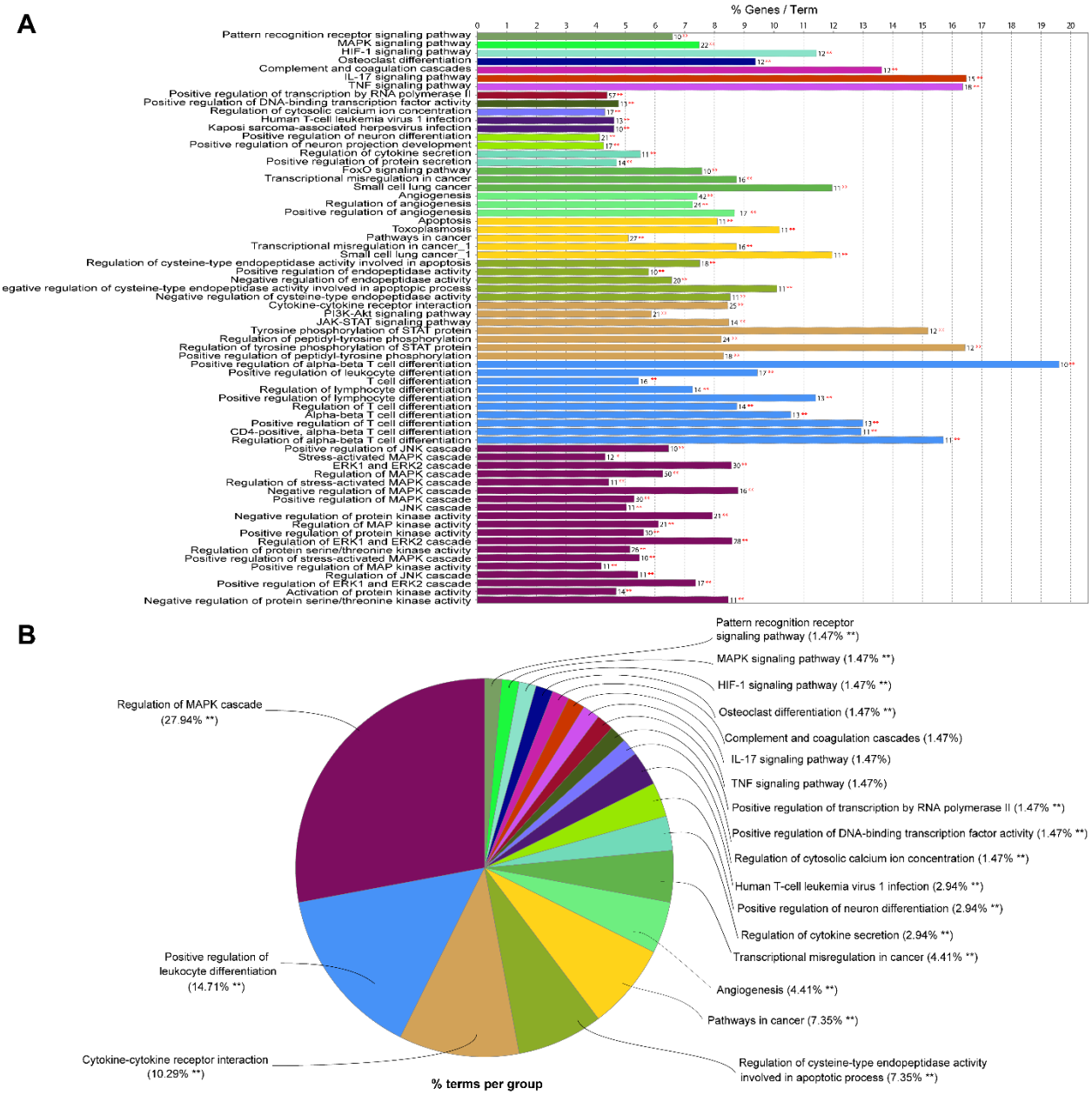

Supplemental Figure 3. Gene Ontology (GO) analysis of differentially expressed genes in CHF+vehicle compared with sham performed using the Cytoscape plugin ClueGO. GO terms represented includes major functional category groupings for biological process and molecular function along with KEGG pathways. A. GO/pathway terms specific for the differentially expressed genes. The bars represent the number of highly expressed genes associated with the terms. B. An overview chart showing the percentage contribution of each enriched functional

group, including specific terms for the differentially expressed genes in CHF compared with sham. Sham group, n=5; CHF+Veh group, n=3.

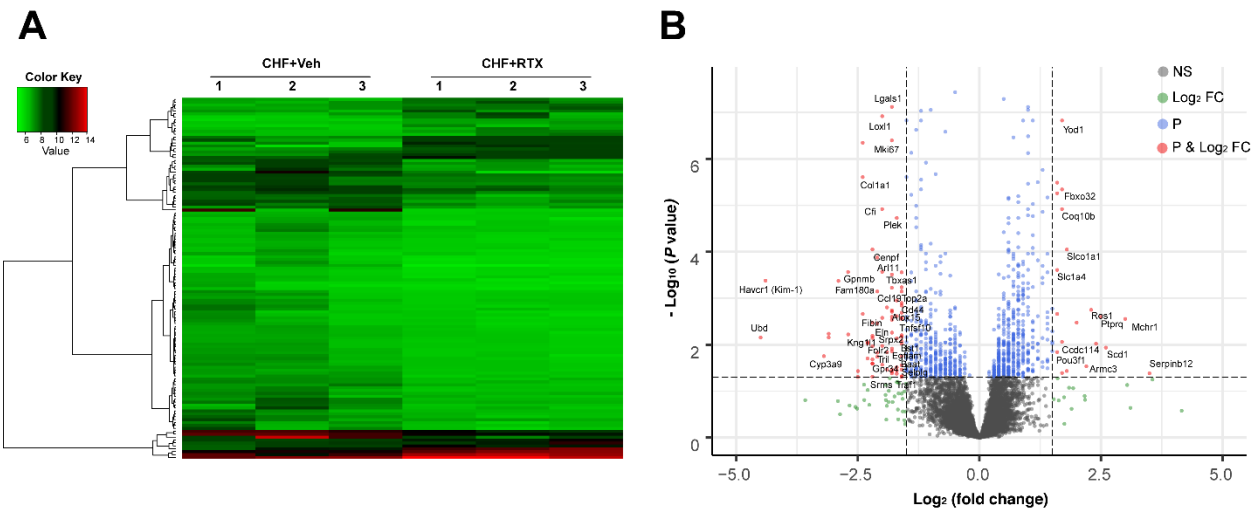

Supplemental Figure 4. A. Heat map of differentially expressed genes extracted from kidneys of CHF+vehicle rats compared with CHF+RTX. Genes were clustered according to their expression profile. Red representing higher level of expression and blue representing lower expression. Gene expression values were converted to *z*-scores to facilitate comparison, and for visual clarity. B. A volcano plot of differentially expressed genes between CHF+vehicle and CHF-RTX rat kidneys. The red dots represent differentially expressed genes with at least 1 $\log_2$ fold-change between CHF compared with CHF+RTX and BH adjusted $P < 0.05$; green and blue dots indicate genes with $\log_2$ fold change ≥1 or Benjamini-Hochberg (BH) adjusted $P \leq 0.05$ respectively. Grey dots indicate genes that had did not meet the cutoff for fold change or *P* value. CHF+Veh group, n=3; CHF+RTX group, n=3.

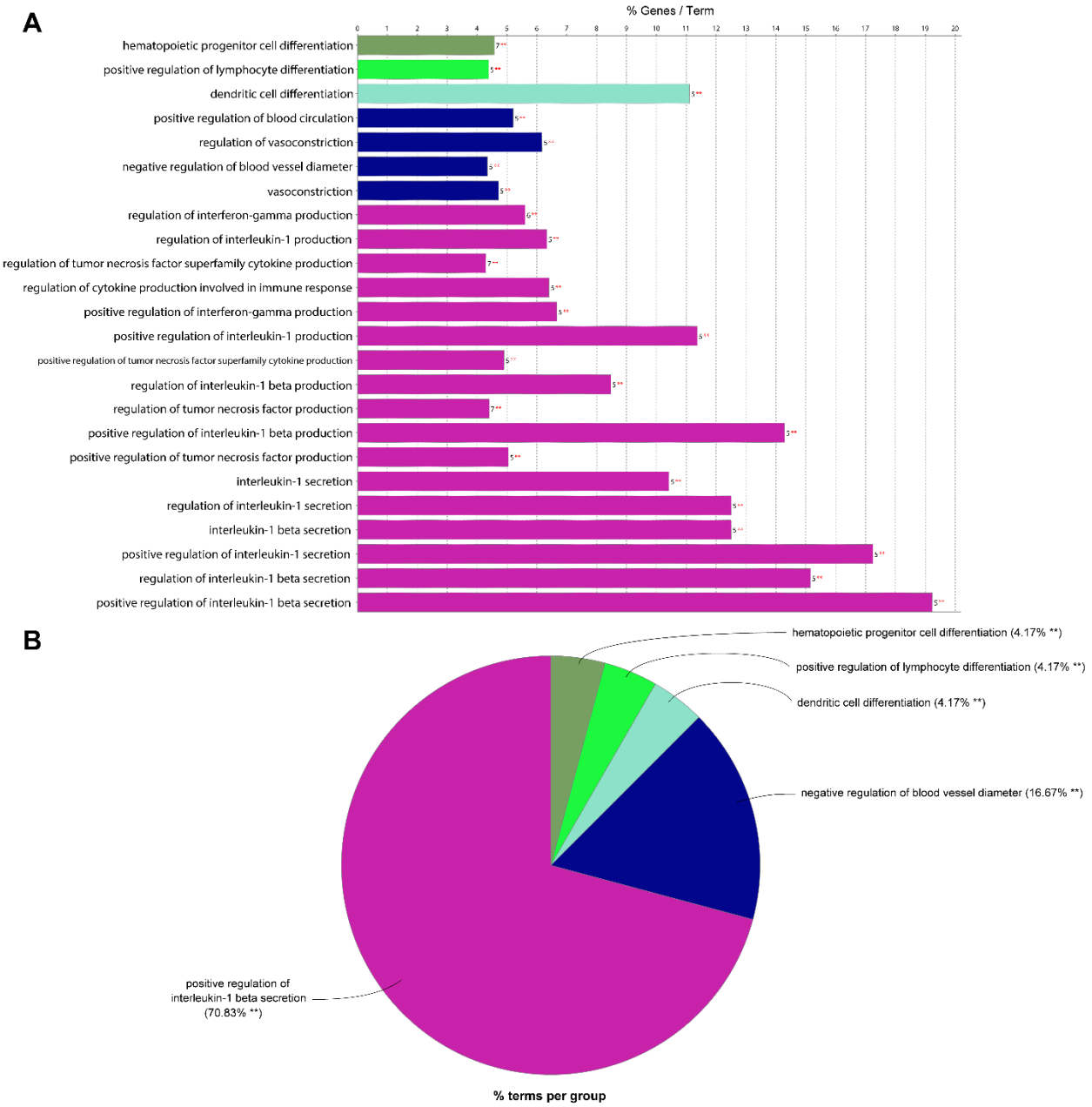

Supplemental Figure 5. Gene Ontology (GO) analysis of differentially expressed genes in CHF+vehicle compared with CHF+RTX performed using the Cytoscape plugin ClueGO. GO terms represented includes major functional category groupings for biological process and molecular function along with KEGG pathways. A. GO/pathway terms specific for the differentially expressed genes. The bars represent the number of highly expressed genes associated with the terms. B. An overview chart showing the percentage contribution of each

enriched functional group, including specific terms for the differentially expressed genes in CHF+vehicle compared with RTX. CHF+Veh group, n=3; CHF+RTX group, n=3.

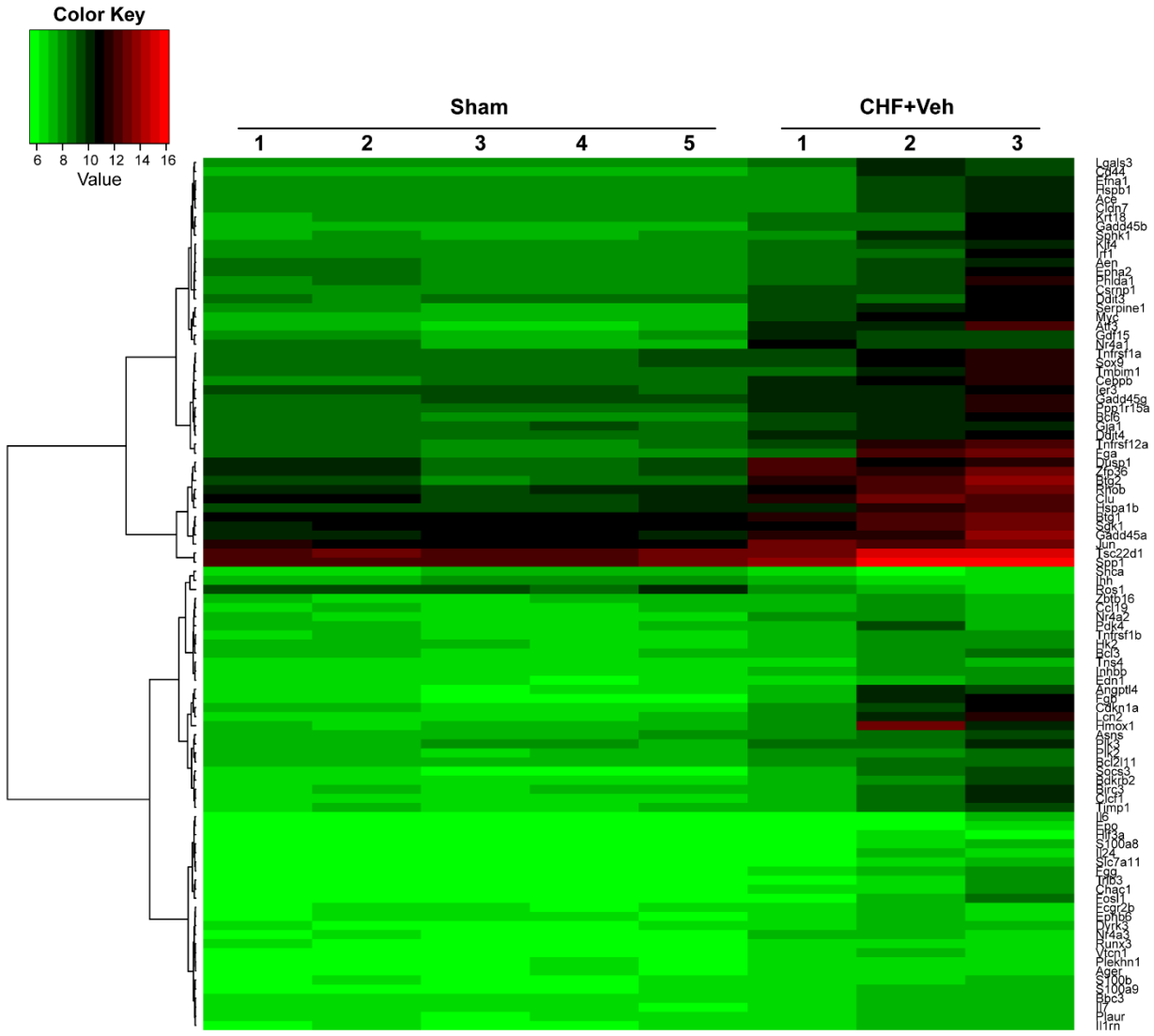

Supplemental Figure 6. Heat map of differentially expressed genes in apoptosis related pathways in kidneys of CHF+vehicle rats compared with sham. Genes were clustered according to their expression profile. Red representing higher level of expression and blue representing lower expression. Gene expression values were converted to *z*-scores to facilitate comparison, and for visual clarity. Sham group, n=5; CHF+Veh group, n=3.

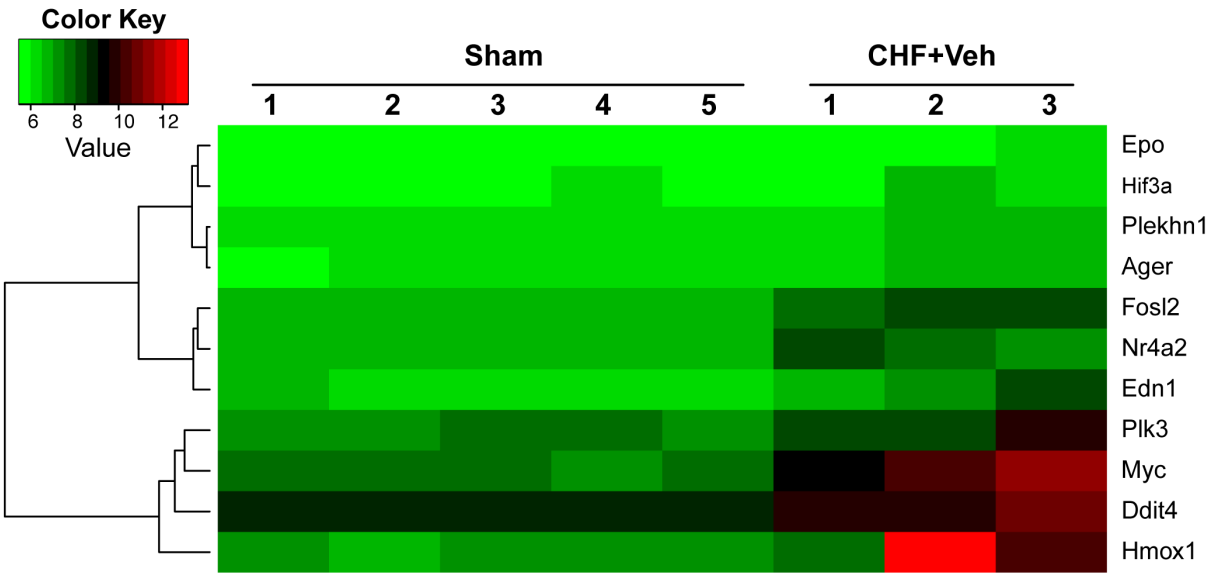

Supplemental Figure 7. Heat map of differentially expressed genes in hypoxia related pathways extracted in kidneys of CHF+vehicle rats compared with sham. Genes were clustered according to their expression profile. Red representing higher level of expression and blue representing lower expression. Gene expression values were converted to *z*-scores to facilitate comparison, and for visual clarity. Sham group, n=5; CHF+Veh group, n=3.

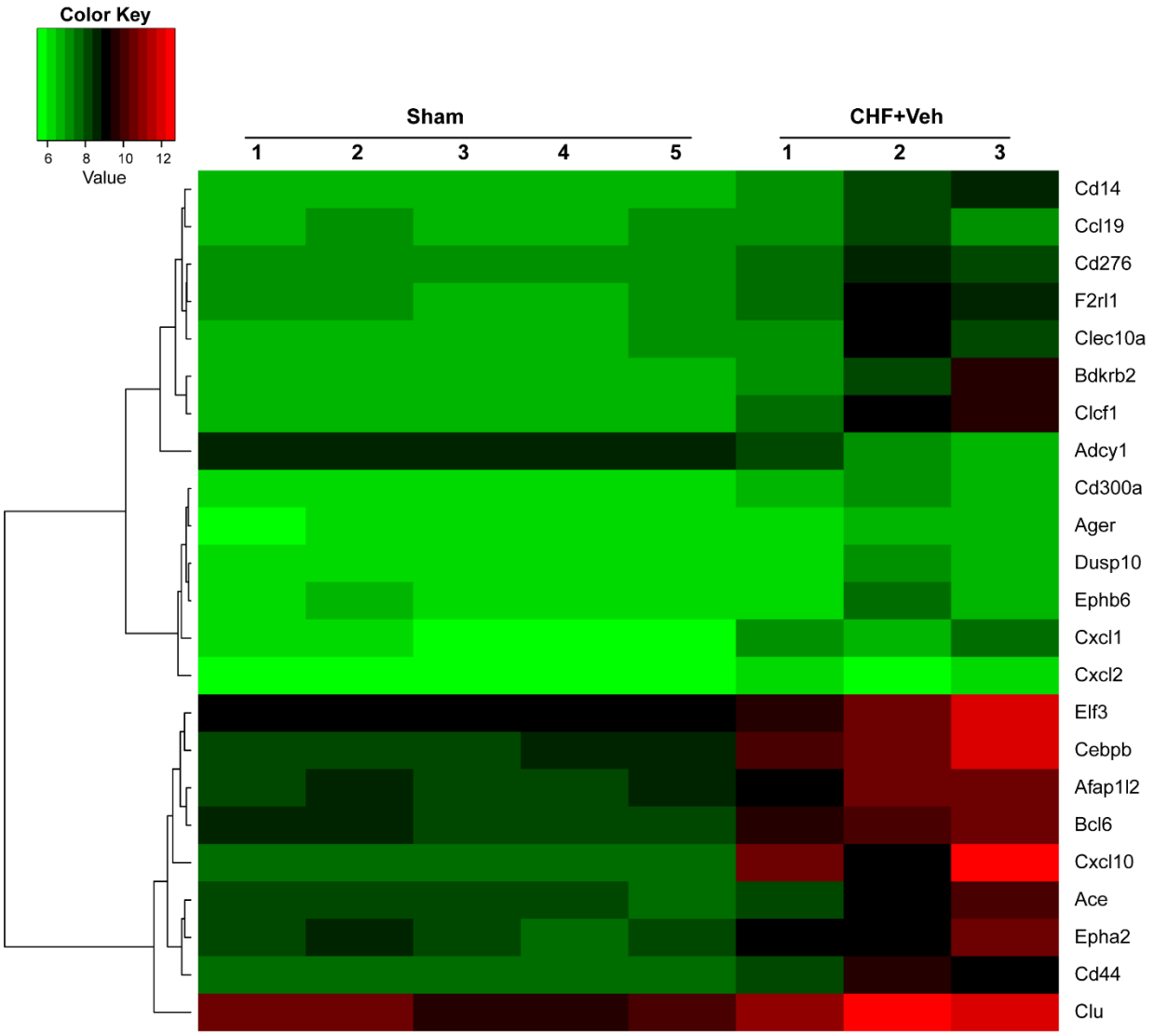

Supplemental Figure 8. Heat map of differentially expressed genes in inflammation pathways in kidneys of CHF+vehicle rats compared with sham. Genes were clustered according to their expression profile. Red representing higher level of expression and blue representing lower expression. Gene expression values were converted to *z*-scores to facilitate comparison, and for visual clarity. Sham group, n=5; CHF+Veh group, n=3.

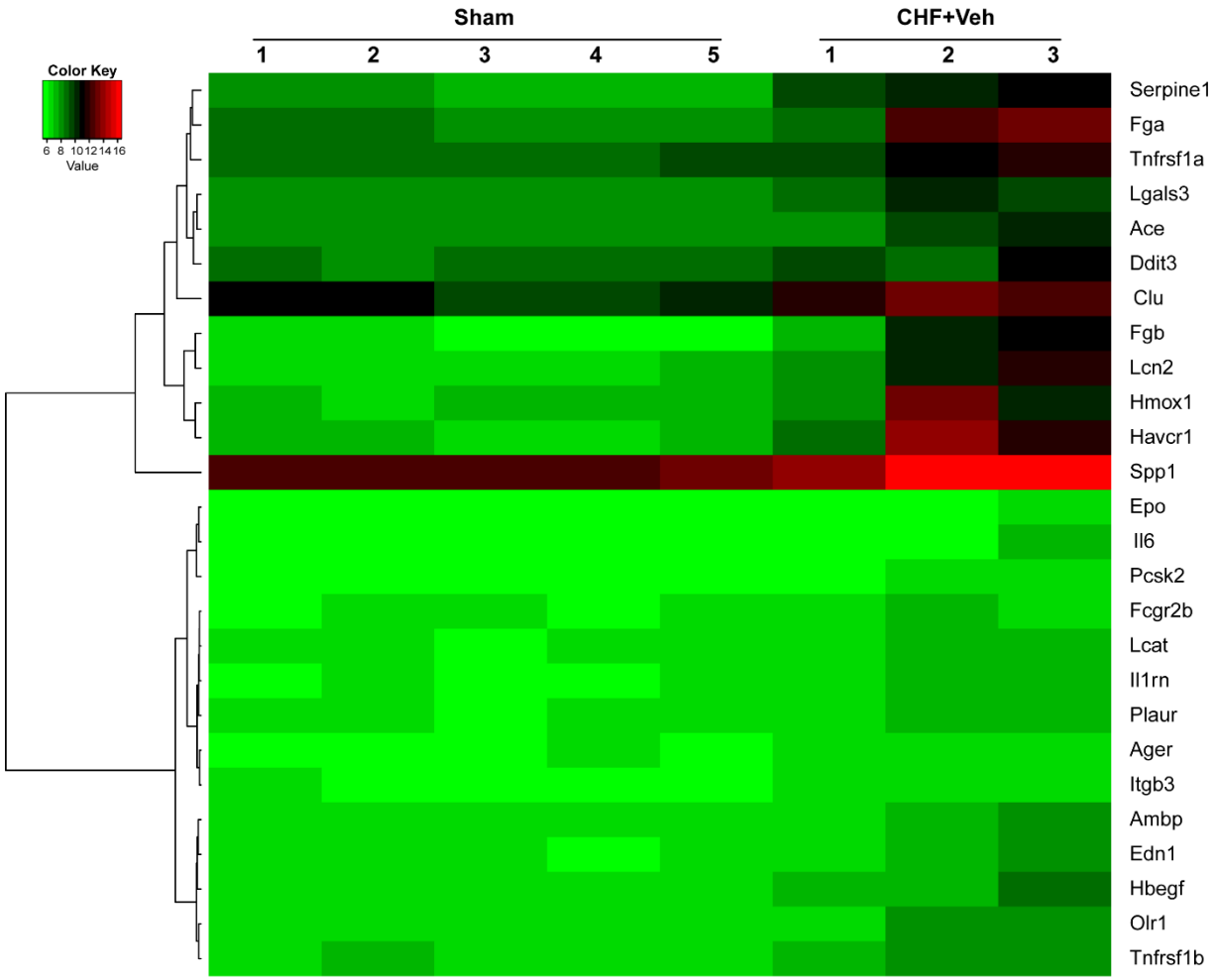

Supplemental Figure 9. Heat map of differentially expressed genes in kidney damage pathways in kidneys of CHF+vehicle rats compared with sham. Genes were clustered according to their expression profile. Red representing higher level of expression and blue representing lower expression. Gene expression values were converted to *z*-scores to facilitate comparison, and for visual clarity. Sham group, n=5; CHF+Veh group, n=3.

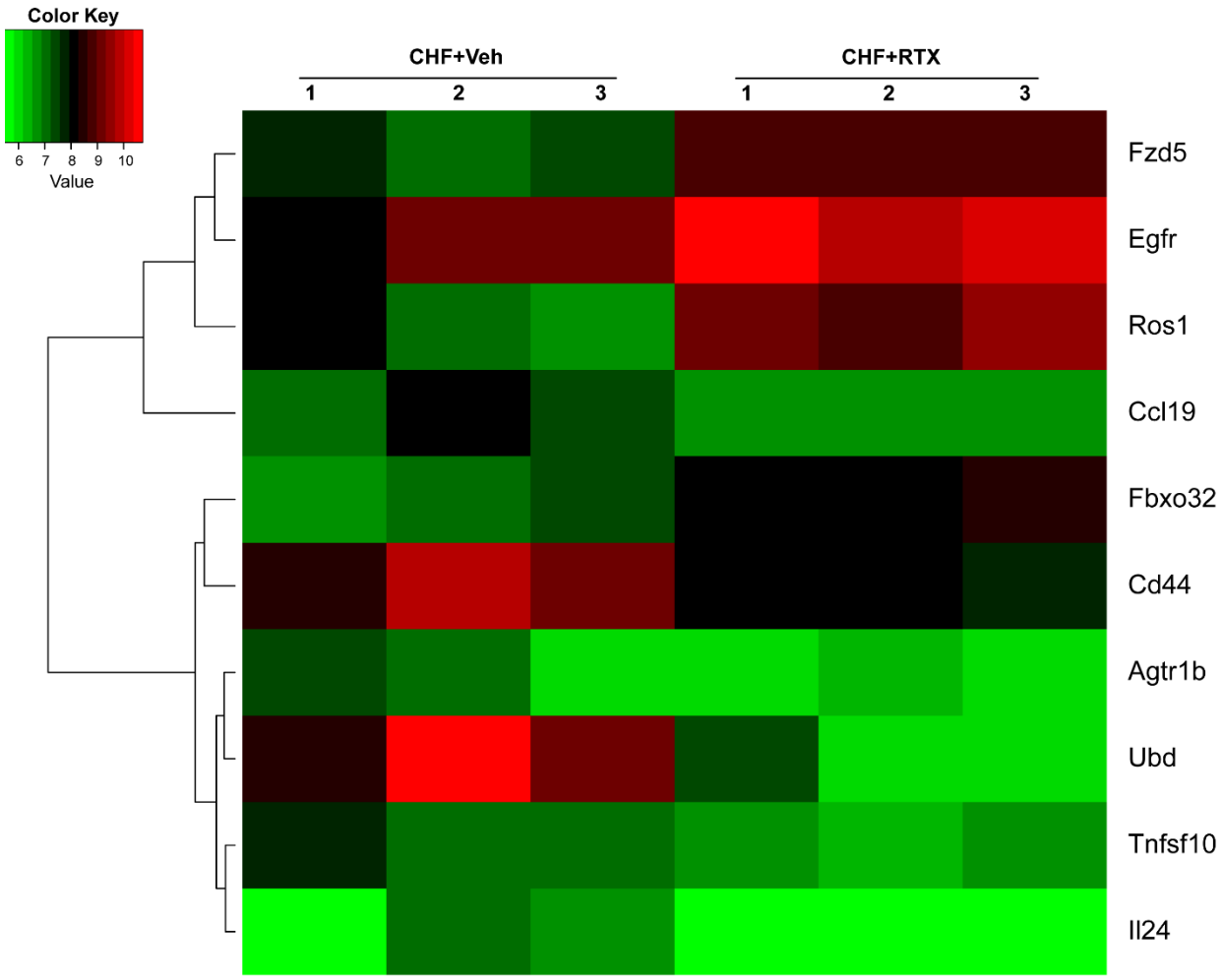

Supplemental Figure 10. Heat map of differentially expressed genes in apoptosis pathways in kidneys of CHF+RTX rats compared with CHF+vehicle treated rats. Genes were clustered according to their expression profile. Red representing higher level of expression and blue representing lower expression. Gene expression values were converted to *z*-scores to facilitate comparison, and for visual clarity. CHF+Veh group, n=3; CHF+RTX group, n=3.

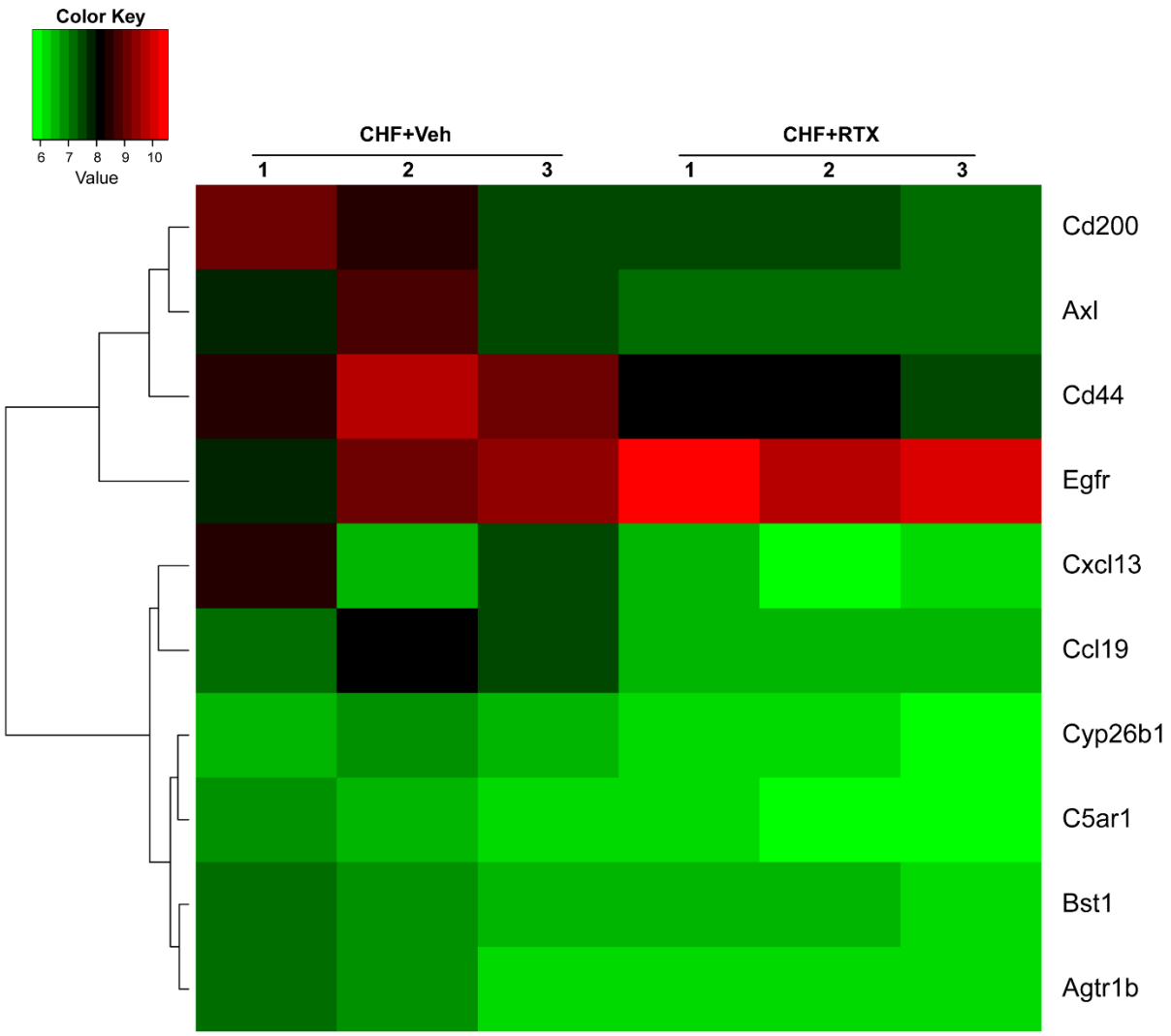

Supplemental Figure 11. Heatmap of differentially expressed genes in inflammation pathways in kidneys of CHF+RTX rats compared with CHF+vehicle treated rats. Genes were clustered according to their expression profile. Red representing higher level of expression and blue representing lower expression. Gene expression values were converted to *z*-scores to facilitate comparison, and for visual clarity. CHF+Veh group, n=3; CHF+RTX group, n=3.

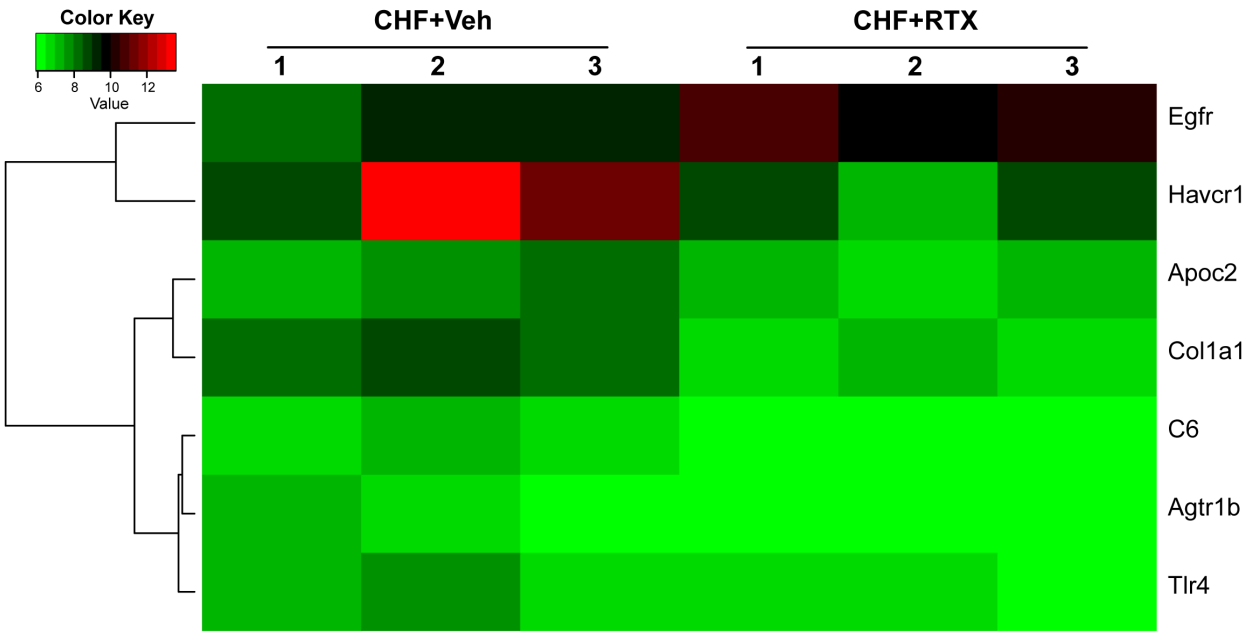

Supplemental Figure 12. Heat map of differentially expressed genes in kidney damage pathways in kidneys of CHF+RTX rats compared with CHF+vehicle treated rats. Genes were clustered according to their expression profile. Red representing higher level of expression and blue representing lower expression. Gene expression values were converted to *z*-scores to facilitate comparison, and for visual clarity. CHF+Veh group, n=3; CHF+RTX group, n=3.

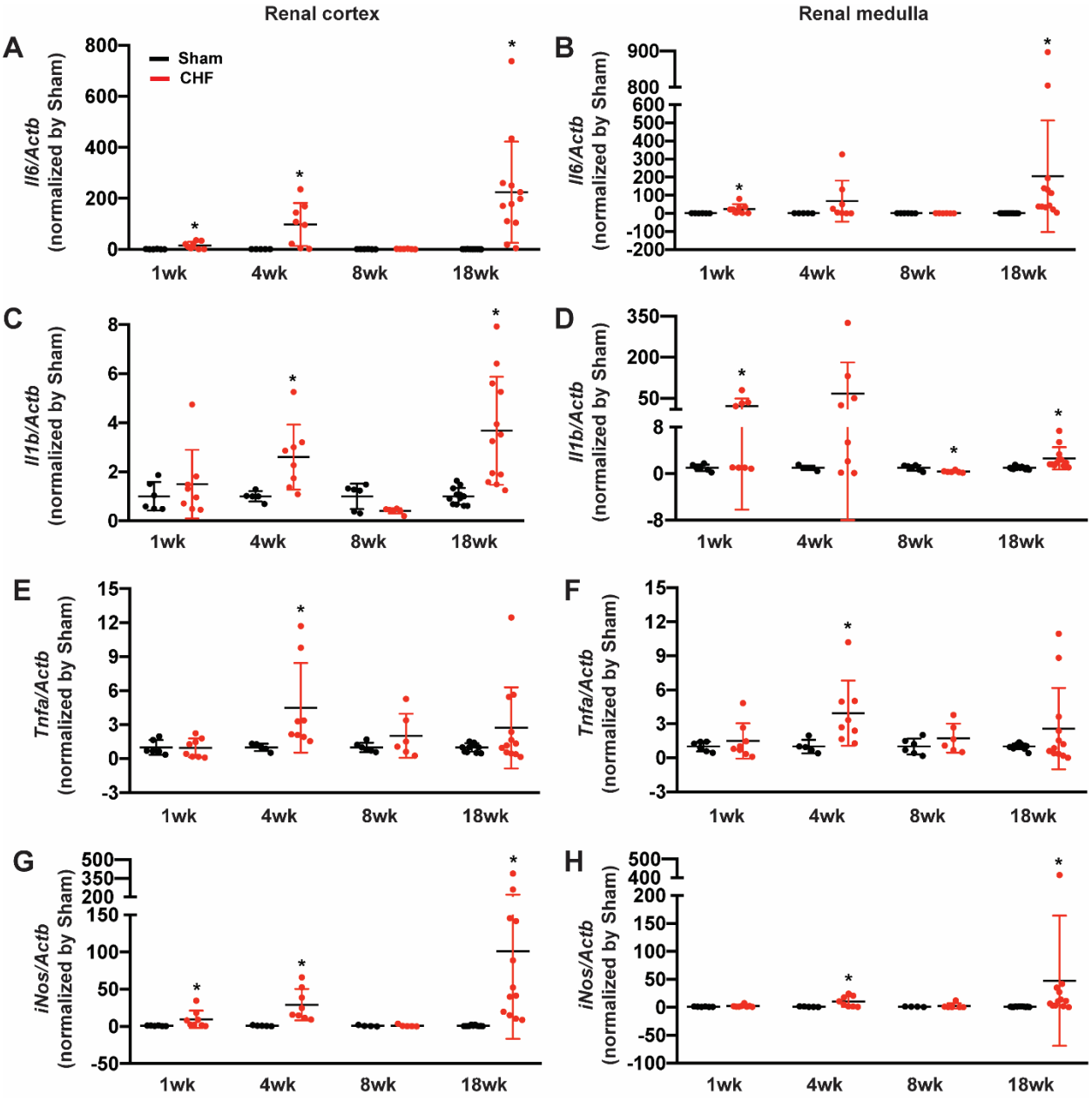

Supplemental Figure 13. Real-time PCR data showing the time-course alteration in the *Il6* (A, B), *Il1b* (C, D), *Tnfa* (E, F), and *iNos* (G, H) mRNA expressions in both renal cortex and medulla from sham and CHF rats. *Il6*, interleukin 6; *Il1b*, interleukin 1beta; *Tnfa*, tumor necrosis factor alpha; *iNos*, inducible nitric oxide synthases; *Actb*, actin beta. A-F. For 1 week, 4 weeks, 8 weeks and 18weeks post-surgery, Sham group, n=6, 5, 6, and 12 respectively; CHF group, n=8, 8, 6, and 12 respectively. G. For 1 week, 4 weeks, 8 weeks and 18weeks post-surgery, Sham group,

n=6, 5, 4, and 11 respectively; CHF group, n=8, 8, 5, and 12 respectively. H. For 1 week, 4 weeks, 8 weeks and 18weeks post-surgery, Sham group, n=6, 5, 4, and 12 respectively; CHF group, n=8, 8, 6, and 12 respectively. *$P < 0.01$ vs Sham.

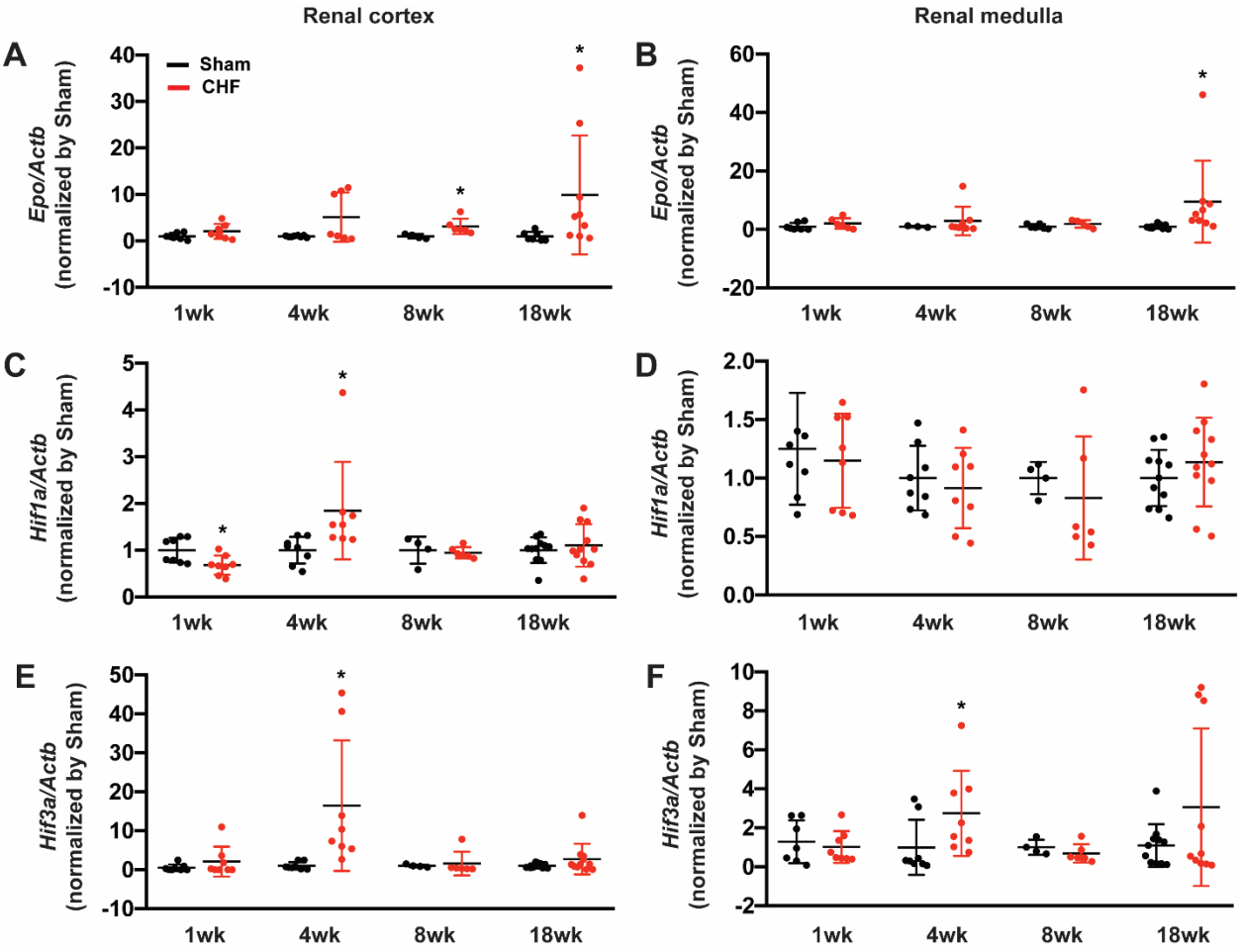

Supplemental Figure 14. Real-time PCR data showing the time-course alteration in the *Epo* (A, b), *Hif1a* (C, D), and *Hif3a* (E, F) mRNA expressions in both renal cortex and medulla from sham and CHF rats. *Epo*, erythropoietin; *Hif1a*, hypoxia-inducible factor 1 alpha; *Hif3a*, hypoxia-inducible factor 3 alpha; *Actb*, actin beta. A. For 1 week, 4 weeks, 8 weeks and 18weeks post-surgery, Sham group, n=7, 8, 4, and 7 respectively; CHF group, n=7, 7, 6, and 9 respectively. B. For 1 week, 4 weeks, 8 weeks and 18weeks post-surgery, Sham group, n=7, 3, 6, and 9 respectively; CHF group, n=6, 8, 5, and 9 respectively. C, D. For 1 week, 4 weeks, 8 weeks and 18weeks post-surgery, Sham group, n=8, 8, 4, and 11 respectively; CHF group, n=8, 8, 6, and 11 respectively. E. For 1 week, 4 weeks, 8 weeks and 18weeks post-surgery, Sham group, n=8, 8, 4, and 10 respectively; CHF group, n=8, 8, 6, and 11 respectively. F. For 1 week,

4 weeks, 8 weeks and 18weeks post-surgery, Sham group, n=7, 8, 4, and 11 respectively; CHF group, n=8, 8, 6, and 10 respectively. *$P < 0.01$ vs Sham.

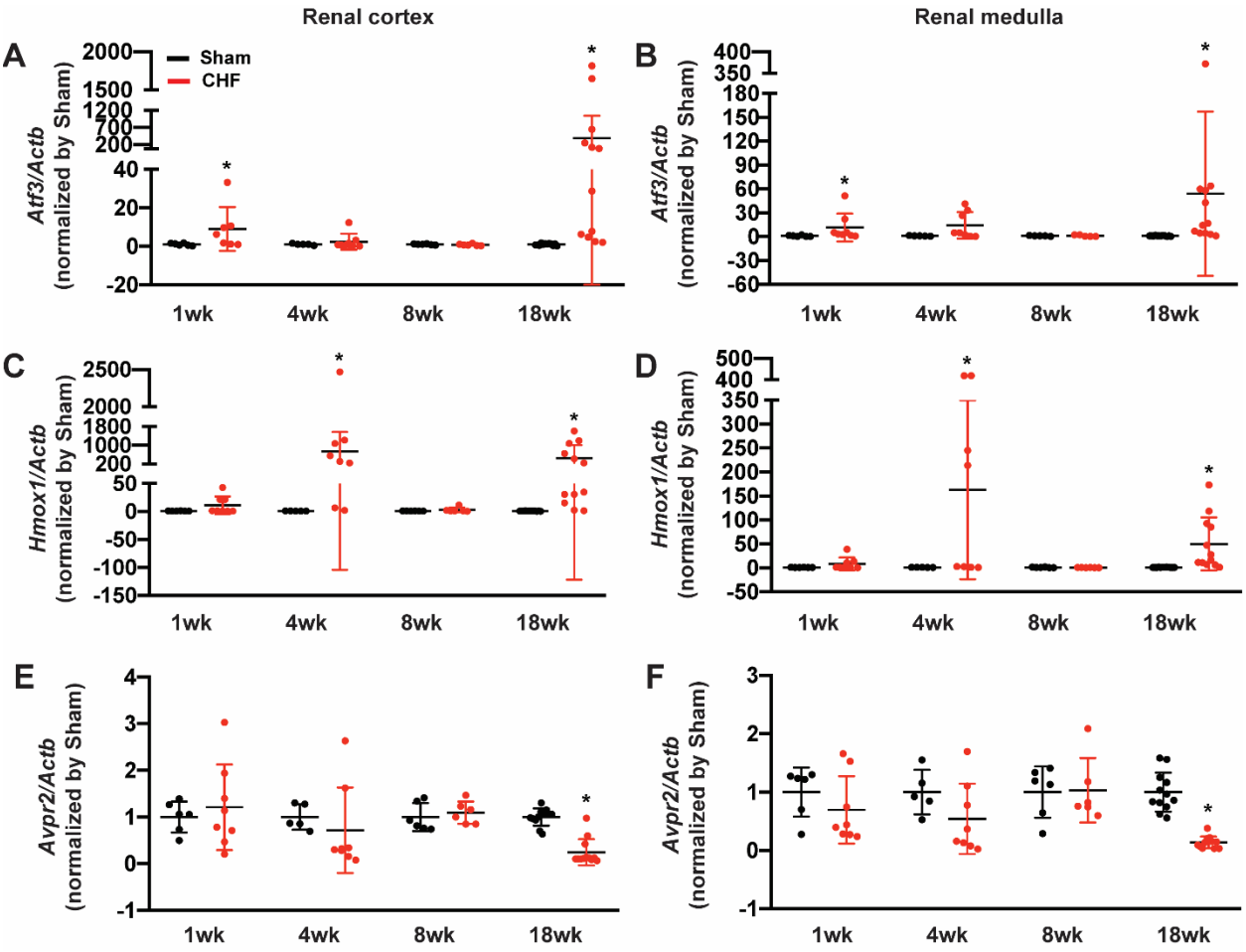

Supplemental Figure 15. Real-time PCR data showing the time-course alteration in the *Atf3* (A, B), *Hmox1* (C, D), and *Avpr2* (E, F) mRNA expressions in both renal cortex and medulla from sham and CHF rats. *Atf3*, activating transcription factor 3; *Hmox1*, heme oxygenase 1; *Avpr2*, arginine vasopressin receptor 2; *Actb*, actin beta. A. For 1 week, 4 weeks, 8 weeks and 18weeks post-surgery, Sham group, n=6, 5, 6, and 12 respectively; CHF group, n=7, 8, 6, and 12 respectively. B. For 1 week, 4 weeks, 8 weeks and 18weeks post-surgery, Sham group, n=6, 5, 5, and 12 respectively; CHF group, n=8, 8, 5, and 12 respectively. C-F. For 1 week, 4 weeks, 8 weeks and 18weeks post-surgery, Sham group, n=6, 5, 6, and 12 respectively; CHF group, n=8, 8, 6, and 12 respectively. *$P < 0.01$ vs Sham.

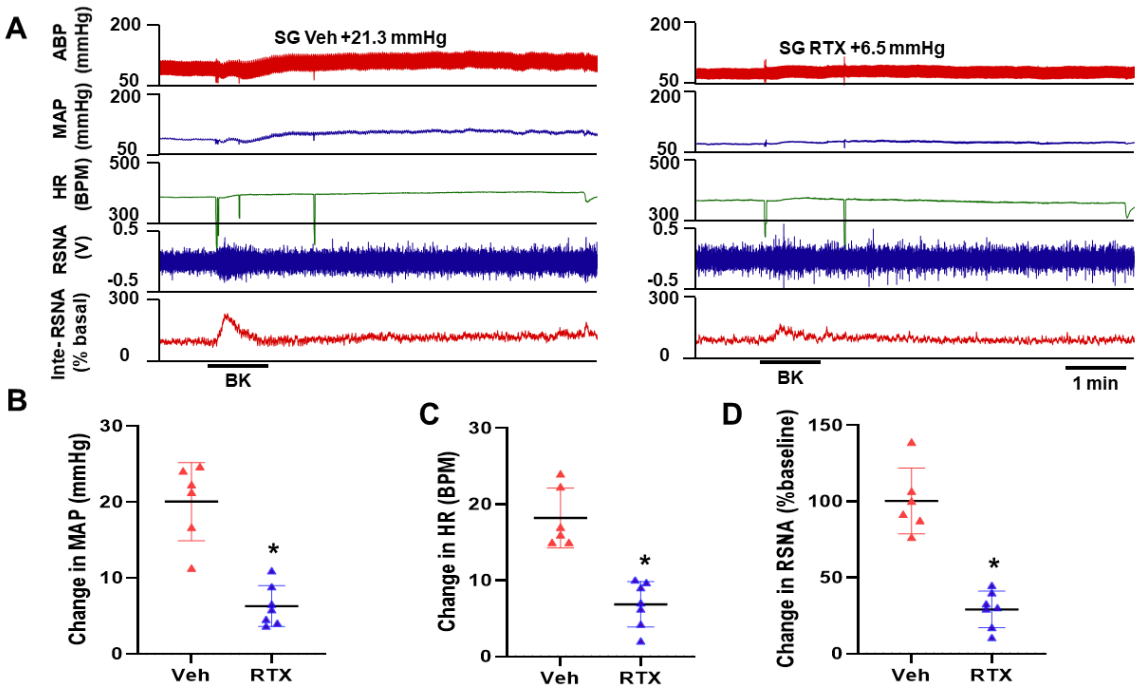

Supplemental Figure 16. (A) Representative recording showing the response to epicardial application of BK (10 µg/mL) in an anesthetized and vagotomized rat. Cardiac spinal afferent reflex (CSAR), arterial blood pressure (ABP), mean arterial blood pressure (MAP), heart rate (HR), renal sympathetic nerve activity (RSNA), integrated RSNA (iRSNA) as a % of baseline. (B) The change in MAP, HR and RSNA from baseline. Data presented as mean ± SD. N=6 for each group. **P* < 0.05 vs SG Veh.

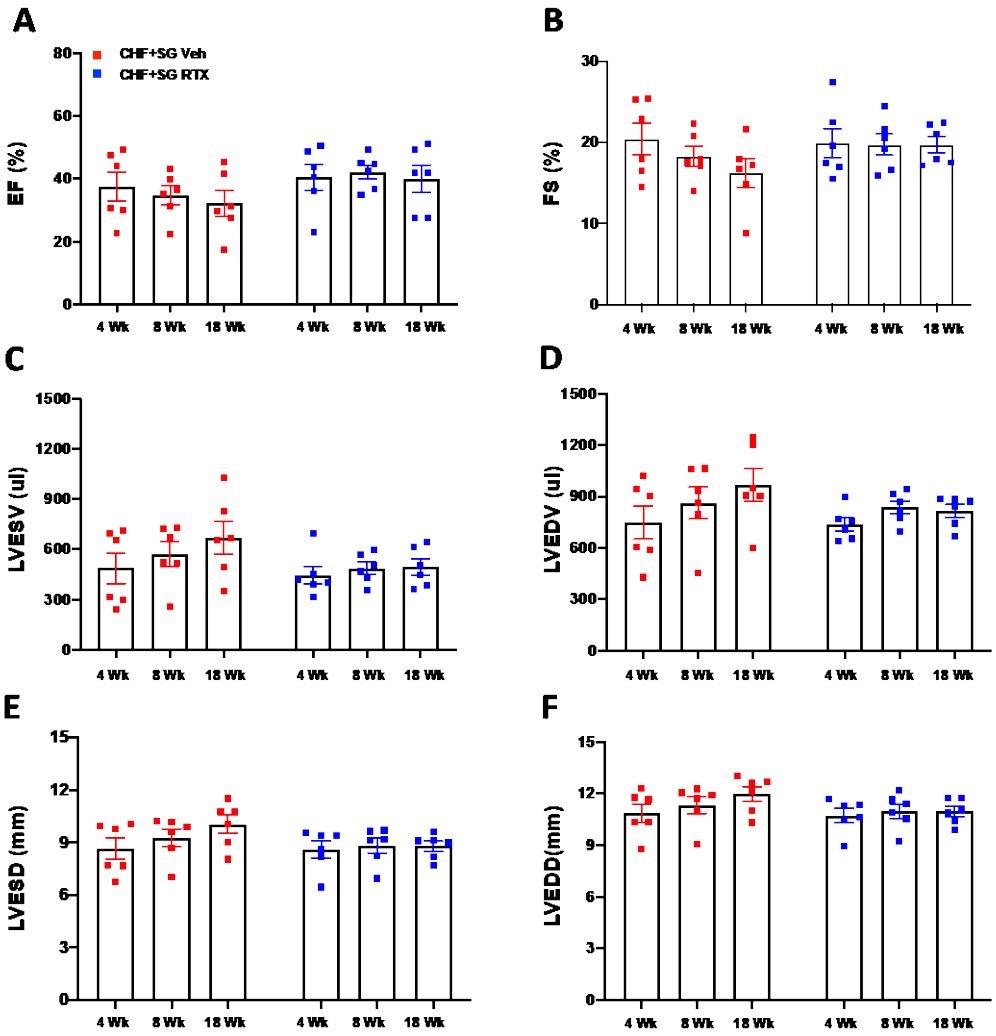

Supplemental Figure 17. Echocardiographic measurements including EF (A), FS (B), LVESV (C), LVEDV (D), LVESD (E), and LVEDD (F) in CHF+SG Veh and CHF+SG RTX rats. CHF+SG Veh group, n=6; CHF+SG RTX group, n=6. EF, ejection fraction; FS, fractional shortening; LVESV, left ventricular end-systolic volume; LVEDV, left ventricular end-diastolic volume; LVESD, left ventricular end-systolic diameter; LVEDD, left ventricular end-diastolic diameter.

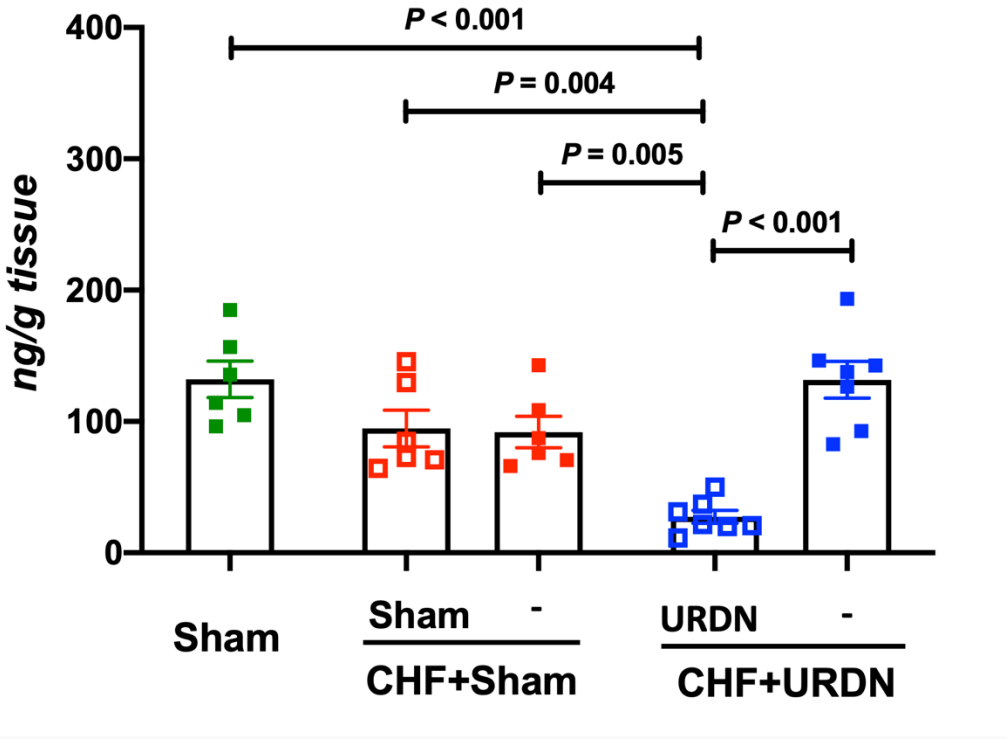

Supplemental Figure 18. Unilateral renal denervation reduced the NE in the denervated kidneys. CHF, chronic heart failure; URDN, unilateral renal denervation; NE, norepinephrine.

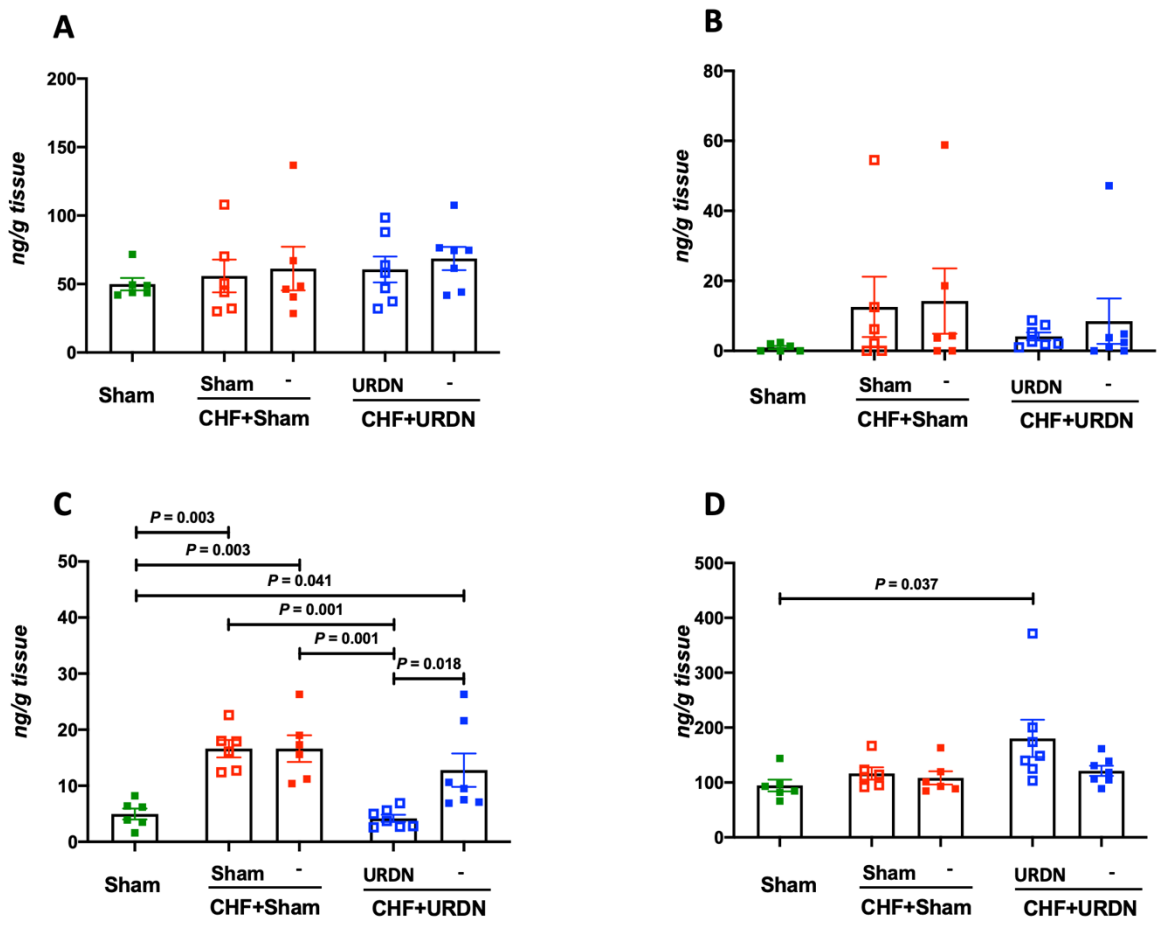

Supplemental Figure 19. The effects of renal denervation on the production of DOPA (A), epinephrine (B), dopamine (C), and serotonin (D) in the kidneys. CHF, chronic heart failure; URDN, unilateral renal denervation.

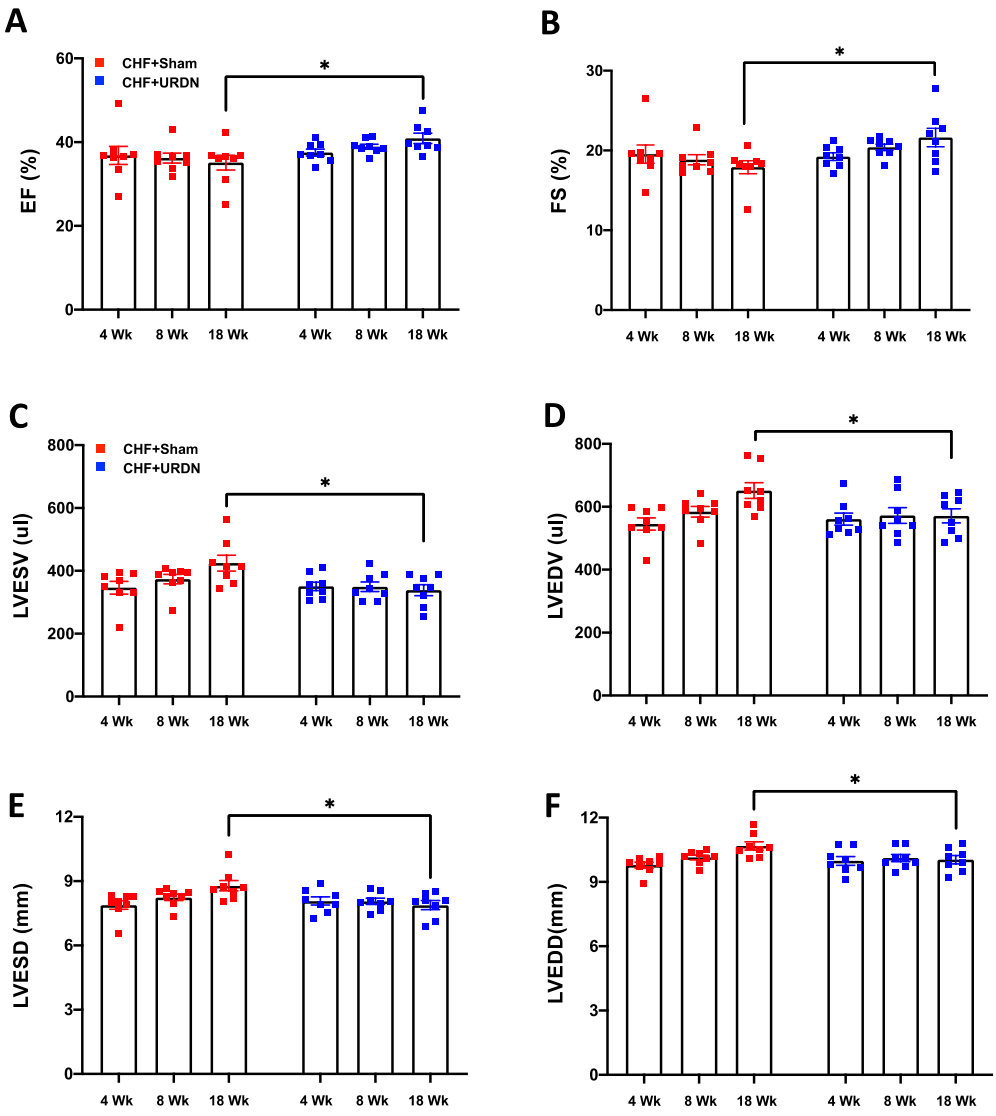

Supplemental Figure 20. Echocardiographic measurements including EF (A), FS (B), LVESV (C), LVEDV (D), LVESD (E), and LVEDD (F) in CHF+Sham and CHF+URDN rats. CHF+Sham group, n=8; CHF+URDN group, n=8. EF, ejection fraction; FS, fractional shortening; LVESV, left ventricular end-systolic volume; LVEDV, left ventricular end-diastolic volume; LVESD, left ventricular end-systolic diameter; LVEDD, left ventricular end-diastolic diameter. *$P < 0.05$ vs CHF+Sham.

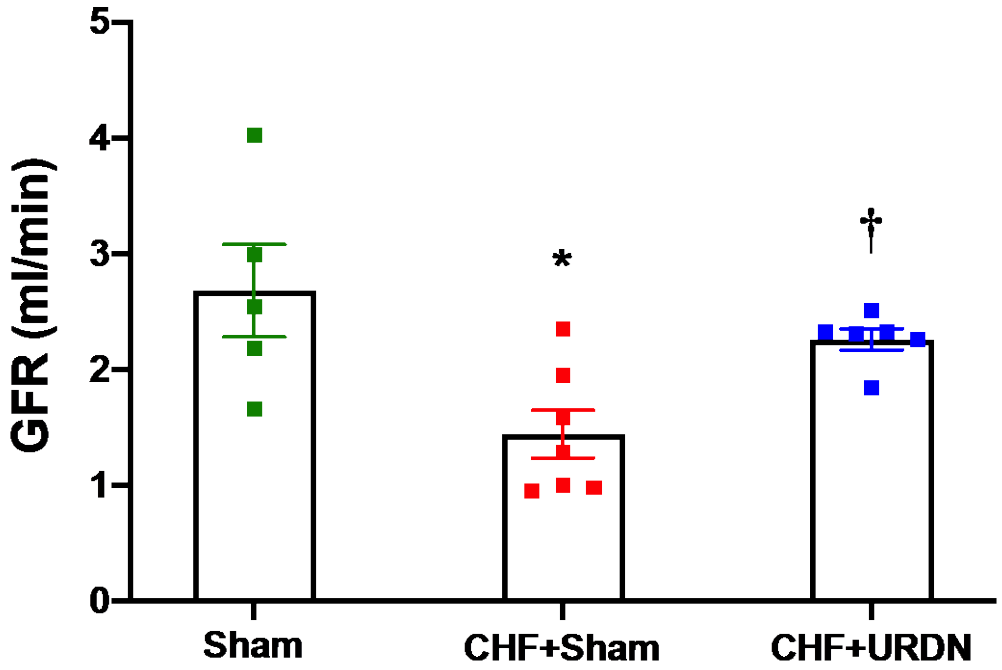

Supplemental Figure 21. Unilateral renal denervation ameliorated renal dysfunction in chronic heart failure. Sham group, n=5; CHF+Sham group, n=7; CHF+URDN, n=6. CHF, chronic heart failure; URDN, unilateral renal denervation. *$P < 0.05$ vs Sham. †$P < 0.05$ vs CHF+Sham.

Supplemental Table 1. Primer Sequences for RT-PCR

Gene	Primer Sequences
Kim1	Forward: 5′-GCC TGG AAT CAC ACT GTA AG-3′
	Reverse: 5′-GCA ACG GAC ATG CCA ACA TAG-3′
Ngal	Forward: 5′-CGA ATG CGG TCC AGA AAG A-3′
	Reverse: 5′-GAG GAT GGA AGT GAC GTT GTA G-3′
Il6	Forward: 5′-TCC TAC CCC AAC TTC CAA TGC TC-3′
	Reverse: 5′-TTG GAT GGT CTT GGT CCT TAG CC-3′
Il1b	Forward: 5′-CAC CTC TCA AGC AGA GCA CAG-3′
	Reverse: 5′-GGG TTC CAT GGT GAA GTC AAC-3′
Actb	Forward: 5′-ACA GGA TGC AGA AGG AGA TTA C-3′
	Reverse: 5′-ACA GTG AGG CCA GGA TAG A-3′
Tnfa	Forward: 5′-AAA TGG GCT CCC TCT ATC AGT TC-3′
	Reverse: 5′-TCT GCT TGG TGG TTT GCT ACG AC-3′
iNos	Forward: 5′-TGG AGC GAG TTG TGG ATT G-3′
	Reverse: 5′-CCT CTT GTC TTT GAC CCA GTA G-3′
Epo	Forward: 5′-CCA GAG AGT CTT CAG CTT CAT ATA G-3′
	Reverse: 5′-TCT GGA GGC GAC ATC AAT TC-3′
Hif1a	Forward: 5′-TCC ATT ACC TGC CTC TGA AAC-3′
	Reverse: 5′-CTC TGG GCT TGA CTC TAA CTT C-3′
Hif3a	Forward: 5′-CAT GGC TTA CCT GTC GGA AA-3′
	Reverse: 5′-CTT GGT CAC AGG GAT GGA TAA A-3′
Atf3	Forward: 5′-GAG ATG CGG TCC AGA GTA TTT C-3′
	Reverse: 5′-TCG GAT TGA ACA CTG AGG ATT T-3′
Hmox1	Forward: 5′-GAT GGC CTC CTT GTA CCA TAT C-3′
	Reverse: 5′-AGC TCC TCA GGG AAG TAG AG-3′
Avpr2	Forward: 5′-GCT CTT CAT CTT TGC TCA GCG T-3′

	Reverse: 5′-TCC AGG TGA CAT AGG CAC GAA-3′

Kim1, kidney injury molecule-1; *Ngal*, neutrophil gelatinase-associated lipocalin; *Il6*, interleukin 6; *Il1b*, interleukin 1beta; *Actb*, actin beta; *Tnfa*, tumor necrosis factor alpha; *iNos*, inducible nitric oxide synthases; *Epo*, erythropoietin; *Hif1a*, hypoxia-inducible factor 1 alpha; *Hif3a*, hypoxia-inducible factor 3 alpha; *Atf3*, activating transcription factor 3; *Hmox1*, heme oxygenase 1; *Avpr2*, arginine vasopressin receptor 2.

Supplemental Table 2. Hemodynamic and Morphologic Data in Sham, CHF+Vehicle, and CHF+RTX Rats That Received iSTAT Measurements

Parameters	Sham (n=8)	CHF+Vehicle (n=14)	CHF+RTX (n=8)
Body weight, g	486 ± 41	499 ± 66	476 ± 40
Heart weight, mg	1355 ± 113	2103 ± 246 *	1608 ± 176 *†
HW/BW, mg/g	2.8 ± 0.3	4.3 ± 0.6 *	3.4 ± 0.5 *†
WLW/BW, mg/g	4.1 ± 0.8	8.8 ± 2.1 *	5.8 ± 1.0 *†
LVESP, mmHg	134.8 ± 6.4	109.2 ± 12.9 *	113.6 ± 11.7 *
LVEDP, mmHg	2.9 ± 2.1	23.8 ± 9.6 *	10.4 ± 2.9*†
EF, %	72.9 ± 2.9	36.4 ± 6.6 *	34.9 ± 7.4 *
FS, %	43.0 ± 2.8	18.1 ± 3.7 *	17.8 ± 3.9 *
Infarct size, %	0	43.1 ± 6.2 *	42.8 ± 3.8*

Values are mean ± SD. BW, body weight; HW, heart weight; WLW, wet lung weight; LVESP, left ventricle end-systolic pressure; LVEDP, left ventricle end-diastolic pressure; EF, ejection fraction; FS, fractional shortening. *$P < 0.05$ vs sham. †$P < 0.05$ vs CHF+Vehicle.

Supplemental Table 3. Baseline Hemodynamic and Morphologic Data in Sham, CHF+Vehicl,e and CHF+RTX Rats Before Acute Activation of Cardiac Sympathetic Afferent Reflex With Bradykinin

Parameters	Sham (n=8)	CHF+Vehicle (n=7)	CHF+RTX (n=7)
Body weight, g	463 ± 25	469 ± 31	460 ± 13
Heart weight, mg	1188 ± 105	2086 ± 236 *	1471 ± 231 *†
HW/BW, mg/g	2.6 ± 0.2	4.4 ± 0.3 *	3.2 ± 0.5 *†
WLW/BW, mg/g	4.2 ± 0.3	8.6 ± 0.9 *	4.4 ± 0.2 †
LVESP, mmHg	135.5 ± 7.6	110.1 ± 8.0 *	118.9 ± 12.3 *
LVEDP, mmHg	3.5 ± 1.5	19.4 ± 3.2 *	8.8 ±3.4 *†
EF, %	73.5 ± 2.5	43.6 ± 4.5 *	40.9± 3.2 *
FS, %	43.1 ± 2.4	22.0± 2.6 *	21.1 ± 2.6 *
Infarct size, %	0	43.0± 4.0 *	46.0± 1.3*

Values are mean ± SD. BW, body weight; HW, heart weight; WLW, wet lung weight; LVESP, left ventricle end-systolic pressure; LVEDP, left ventricle end-diastolic pressure; EF, ejection fraction; FS, fractional shortening. *$P < 0.05$ vs sham. †$P < 0.05$ vs CHF+Vehicle.

Supplemental Table 4. Differentially Expressed Genes Between CHF+Veh and Sham

Gene	log2 Fold Change	*P* value	*P* adj	Direction
Prss22	8.0	2.08E-07	1.09E-05	up
Tgm1	7.2	1.43E-08	1.19E-06	up
Fosl1	7.2	2.55E-09	2.63E-07	up
Lypd8	7.2	2.14E-05	4.70E-04	up
Havcr1	6.7	9.03E-15	3.26E-12	up
Il1r2	6.3	4.97E-09	4.76E-07	up
Fgb	6.1	5.56E-11	8.36E-09	up
Csf3	6.1	4.87E-05	8.85E-04	up
Ugt1a2	5.9	8.05E-08	4.95E-06	up
Il24	5.8	1.4E-05	3.41E-04	up
Hmox1	5.8	4.15E-09	4.02E-07	up
Serpina3n	5.7	1.83E-12	4.13E-10	up
Mfsd2a	5.7	3.94E-06	1.25E-04	up
Vgf	5.6	2.6E-06	9.18E-05	up
LOC298795	5.6	1.69E-12	3.9E-10	up
Igfbp1	5.4	3.76E-17	2.55E-14	up
Il6	5.3	1.44E-05	3.48E-04	up
Atf3	5.3	8.67E-38	9.39E-34	up
Lcn2	5.2	5.03E-14	1.6E-11	up
Rasd1	5.0	6.53E-17	3.93E-14	up
Slc7a11	5.0	3.63E-08	2.5E-06	up
Fgg	5.0	1.36E-10	1.78E-08	up
Trim15	4.9	1.5E-05	3.59E-04	up
Lamc2	4.8	8.18E-15	3.05E-12	up
Trib3	4.8	5.04E-06	1.52E-04	up
Socs3	4.8	4.1E-23	6.34E-20	up
Trpv6	4.7	6.18E-09	5.8E-07	up
Adamts4	4.6	5.81E-10	6.84E-08	up
Rnd1	4.6	2.61E-16	1.41E-13	up
PVR	4.5	1.03E-11	1.82E-09	up
Fosb	4.5	4.03E-06	1.27E-04	up
Btg2	4.5	5.89E-14	1.75E-11	up
Angptl4	4.4	1.25E-08	1.04E-06	up
Chac1	4.4	2.25E-06	8.13E-05	up
Cdkn1a	4.4	2.09E-20	2.84E-17	up
Cxcl10	4.4	4.43E-12	9.04E-10	up
Fga	4.3	1.07E-08	9.02E-07	up
Lif	4.3	4.61E-07	2.21E-05	up
Glycam1	4.3	3.46E-12	7.21E-10	up
Cxcl2	4.2	2.90E-04	0.003	up
Nfil3	4.2	3.18E-18	2.87E-15	up
Arid5a	4.2	3.54E-17	2.55E-14	up
Cyp3a9	4.1	1.9E-06	7.02E-05	up
Bcat1	4.1	6.74E-12	1.28E-09	up
Cldn4	3.9	1.26E-10	1.68E-08	up
S100a8	3.9	2.63E-06	9.23E-05	up
RGD1564664	3.9	2.36E-10	2.93E-08	up
Cxcl1	3.9	1.11E-10	1.5E-08	up
Cbarp	3.7	3.77E-14	1.28E-11	up
Myc	3.7	6.52E-28	1.77E-24	up

Pcsk1	3.6	4.07E-08	2.74E-06	up
Cfd	3.5	1.6E-06	6.11E-05	up
Epo	3.5	0.003	0.018	up
Lexm	3.5	1.70E-04	0.002	up
Cebpd	3.5	5.91E-24	1.07E-20	up
Clcf1	3.5	1.2E-12	2.88E-10	up
Serpine1	3.5	6.41E-14	1.83E-11	up
Bdkrb2	3.5	8.02E-10	8.96E-08	up
B4galnt4	3.5	1.8E-07	9.74E-06	up
Il23a	3.4	5.89E-05	0.001	up
Apold1	3.4	1.14E-19	1.37E-16	up
Tnfrsf12a	3.3	6.31E-08	4E-06	up
Nfkbiz	3.3	1.14E-13	3.08E-11	up
Tubb6	3.3	4.1E-09	4E-07	up
Birc3	3.3	3.43E-14	1.2E-11	up
Cyp3a9	3.3	1.87E-07	1.01E-05	up
Ptx3	3.3	5.78E-05	0.001	up
A2m	3.3	1.81E-04	0.002	up
Map3k6	3.2	1.64E-12	3.87E-10	up
Rgs1	3.2	5.88E-16	3.03E-13	up
Osmr	3.2	3.15E-13	8.13E-11	up
Spp1	3.2	4.58E-18	3.82E-15	up
Sphk1	3.1	4.75E-11	7.36E-09	up
Gadd45b	3.1	2.18E-10	2.77E-08	up
Maff	3.0	1.07E-15	5.04E-13	up
Nr4a3	3.0	6.63E-12	1.28E-09	up
Cebpb	3.0	7.31E-19	7.92E-16	up
Hbegf	3.0	7.49E-11	1.07E-08	up
LOC684871	3.0	8.58E-14	2.38E-11	up
Pcsk2	3.0	0.001	0.011	up
Lax1	2.9	1.86E-04	0.002	up
S100a9	2.9	1.22E-07	7.01E-06	up
Gpnmb	2.9	8.92E-09	7.92E-07	up
Socs1	2.9	2.28E-08	1.74E-06	up
Tmem252	2.8	3.57E-15	1.43E-12	up
Sds	2.8	3.14E-06	1.05E-04	up
Anxa8	2.8	6.77E-05	0.001	up
Tgif1	2.8	4.64E-15	1.79E-12	up
Srxn1	2.8	1.33E-05	3.27E-04	up
Klf6	2.8	1.02E-12	2.5E-10	up
Zfp36	2.8	2.55E-17	1.98E-14	up
Ctgf	2.7	5.66E-07	2.62E-05	up
Hif3a	2.7	0.004	0.022	up
Upp1	2.7	3.41E-10	4.15E-08	up
Ucma	2.7	8.3E-07	3.48E-05	up
Dusp2	2.7	6.75E-05	0.001	up
Dmbt1	2.7	3.77E-07	1.86E-05	up
Edn1	2.6	6.91E-09	6.34E-07	up
Slc16a3	2.6	5.67E-10	6.74E-08	up
Csrnp1	2.6	2.68E-15	1.11E-12	up
Timp1	2.6	9.46E-11	1.3E-08	up
Chi3l1	2.6	0.001	0.010	up
Kng1l1	2.6	3.97E-05	7.61E-04	up

Il1rn	2.6	1.83E-08	1.44E-06	up
Gdf15	2.5	1.43E-31	6.16E-28	up
Ccnf	2.5	5.22E-05	9.31E-04	up
Selp	2.5	2.83E-04	0.003	up
Fam46b	2.5	7.86E-04	0.007	up
Ptprz1	2.5	3.73E-06	1.19E-04	up
Lrg1	2.5	1.67E-07	9.32E-06	up
Rab7b	2.5	1.05E-04	0.002	up
Fam167a	2.5	2.68E-08	2.01E-06	up
Itpkc	2.5	2.9E-08	2.15E-06	up
Krt18	2.5	1.95E-08	1.52E-06	up
Slc7a1	2.5	2.11E-08	1.62E-06	up
C4b	2.5	8.77E-17	5E-14	up
Gadd45a	2.5	2.76E-06	9.61E-05	up
Dusp1	2.5	6.27E-13	1.58E-10	up
Egr2	2.5	2.81E-05	5.80E-04	up
Hspa1a	2.4	3.46E-08	2.45E-06	up
Cyp11a1	2.4	0.001	0.009	up
Mt2A	2.4	3.32E-11	5.37E-09	up
Phlda1	2.4	9.3E-05	0.001	up
Vtcn1	2.4	1.11E-07	6.49E-06	up
Gpx2	2.4	0.003	0.020	up
Crtac1	2.4	6.23E-06	1.78E-04	up
Fkbp5	2.4	2.7E-12	5.84E-10	up
Gem	2.3	5.71E-14	1.75E-11	up
Fam25a	2.3	3.26E-04	0.004	up
Gprc5a	2.3	2.73E-09	2.77E-07	up
Clec10a	2.3	2.44E-06	8.67E-05	up
Arl4c	2.3	9.13E-12	1.7E-09	up
Fam129a	2.3	5.88E-11	8.64E-09	up
F2rl1	2.3	1.49E-08	1.22E-06	up
Car3	2.3	0.003	0.021	up
Ifnlr1	2.3	0.003	0.017	up
Afap1l2	2.3	1.08E-09	1.17E-07	up
Pou3f1	2.3	7.87E-08	4.87E-06	up
Map1b	2.3	9.59E-05	0.001	up
Mex3b	2.3	5.05E-05	9.11E-04	up
Prg4	2.3	5.32E-07	2.48E-05	up
Slc7a5	2.3	9.97E-06	2.62E-04	up
LOC500300	2.3	4.7E-17	2.99E-14	up
Elf3	2.3	6.25E-09	5.8E-07	up
Inhbb	2.3	5.45E-11	8.31E-09	up
Pnrc1	2.3	1.78E-15	7.7E-13	up
Cd14	2.3	3.89E-09	3.87E-07	up
Fosl2	2.2	9.25E-12	1.7E-09	up
Nr4a1	2.2	4.27E-04	0.005	up
Eid3	2.2	0.002	0.016	up
Ppp1r15a	2.2	1.41E-13	3.71E-11	up
Nyap1	2.2	3.23E-08	2.35E-06	up
Penk	2.2	0.003	0.020	up
Pla1a	2.2	9.47E-08	5.73E-06	up
Nfkbia	2.2	8.21E-28	1.78E-24	up
Hspa1b	2.2	1.05E-09	1.15E-07	up

Scel	2.2	3.42E-05	6.79E-04	up
Cd44	2.2	1.88E-11	3.27E-09	up
Plin2	2.2	6.82E-05	0.001	up
Dusp5	2.2	4.48E-08	2.98E-06	up
Rhob	2.2	1.9E-11	3.27E-09	up
Sox9	2.2	1.34E-07	7.64E-06	up
Bcl3	2.2	5E-06	1.51E-04	up
Ier5	2.2	5.15E-12	1.02E-09	up
Akap12	2.2	2.28E-07	1.19E-05	up
Chka	2.2	1.62E-08	1.31E-06	up
Plk3	2.2	3.63E-08	2.5E-06	up
Col7a1	2.1	3.24E-05	6.48E-04	up
RT1-CE6	2.1	3.07E-04	0.004	up
Gpr4	2.1	5.69E-07	2.62E-05	up
Lypd3	2.1	2.19E-06	7.93E-05	up
Ldlr	2.1	3.25E-08	2.35E-06	up
Nr4a2	2.1	7.6E-11	1.07E-08	up
S100b	2.1	8.88E-04	0.008	up
S100a10	2.1	2.08E-09	2.17E-07	up
Pthlh	2.1	1.36E-04	0.002	up
Mab21l3	2.1	6.22E-11	8.98E-09	up
Dyrk3	2.1	1.78E-04	0.002	up
Gzmk	2.1	7.84E-05	0.001	up
Spsb1	2.1	6.33E-07	2.84E-05	up
Gpsm1	2.1	4.55E-05	8.42E-04	up
Arntl	2.1	6.8E-05	0.001	up
Clu	2.1	6.7E-10	7.8E-08	up
Tsc22d1	2.1	6.81E-10	7.85E-08	up
Tinagl1	2.0	6.32E-08	4E-06	up
Creb5	2.0	6.77E-04	0.006	up
Fgl2	2.0	2.88E-07	1.44E-05	up
Cldn7	2.0	9.74E-08	5.86E-06	up
Uchl1	2.0	3.78E-05	7.33E-04	up
Runx1	2.0	9.81E-07	4.06E-05	up
Akr1b8	2.0	7.9E-05	0.001	up
Epha2	2.0	1.09E-07	6.43E-06	up
Ier2	2.0	2.05E-10	2.65E-08	up
Klf4	2.0	2.07E-06	7.54E-05	up
Bhlha15	2.0	8.24E-04	0.007	up
Gnat1	2.0	1.34E-05	3.29E-04	up
Arl4a	2.0	6E-14	1.75E-11	up
Bcl6	2.0	3.93E-11	6.25E-09	up
Adamts1	2.0	1.72E-08	1.37E-06	up
Cxcr4	2.0	1.08E-07	6.39E-06	up
Fcgr2b	2.0	9.21E-06	2.47E-04	up
Sh2b2	2.0	2.79E-05	5.76E-04	up
Rnf125	2.0	1.51E-05	3.62E-04	up
Tmbim1	2.0	1.45E-06	5.65E-05	up
Klf5	2.0	5.76E-07	2.64E-05	up
Junb	2.0	7.75E-08	4.82E-06	up
Fam84a	2.0	2.75E-07	1.39E-05	up
Ddit4l2	2.0	4.13E-04	0.005	up
Plaur	2.0	3.25E-04	0.004	up

Mt1a	1.9	2.14E-12	4.74E-10	up
Isg20	1.9	1.83E-04	0.002	up
Pdk4	1.9	6.45E-04	0.006	up
Gpr171	1.9	6.63E-16	3.26E-13	up
Il7	1.9	5.42E-06	1.60E-04	up
Mrc1	1.9	3.71E-06	1.19E-04	up
Sat1	1.9	2.41E-07	1.23E-05	up
Alox15	1.9	1.77E-07	9.71E-06	up
Sh2d2a	1.9	2.4E-05	5.12E-04	up
Ephb6	1.9	8.14E-04	0.007	up
Slc5a3	1.9	2.31E-06	8.24E-05	up
Map3k8	1.9	3.98E-07	1.95E-05	up
P2ry10	1.9	7.95E-09	7.17E-07	up
Itgb3	1.9	1.76E-06	6.63E-05	up
Jun	1.9	5.18E-12	1.02E-09	up
Lgals3	1.9	1.13E-07	6.56E-06	up
Sbno2	1.9	3.99E-07	1.95E-05	up
Tnfrsf1b	1.9	3.52E-08	2.48E-06	up
Dusp8	1.9	8.03E-07	3.41E-05	up
Nov	1.9	3.65E-04	0.004	up
Irf1	1.9	3.89E-05	7.48E-04	up
Slc20a1	1.9	4.31E-06	1.34E-04	up
Slfn2	1.8	2.34E-05	5.03E-04	up
Angptl8	1.8	0.006	0.032	up
Pdlim1	1.8	6.57E-06	1.86E-04	up
Tnfrsf1a	1.8	6.2E-08	3.97E-06	up
Il6r	1.8	1.02E-08	8.7E-07	up
RGD1305807	1.8	3.72E-04	0.004	up
Ptges	1.8	4.93E-06	1.50E-04	up
Asns	1.8	2.58E-05	5.42E-04	up
Olr1	1.8	6.8E-06	1.91E-04	up
Mss51	1.8	5.2E-05	9.31E-04	up
Sema6b	1.8	1.17E-05	2.95E-04	up
Cyr61	1.8	3.2E-05	6.42E-04	up
Minpp1	1.8	3.7E-06	1.19E-04	up
Dnajb3	1.8	8.36E-06	2.27E-04	up
Cfi	1.8	9.89E-09	8.5E-07	up
Cd3eap	1.8	2.64E-05	5.51E-04	up
Tifa	1.8	1.94E-06	7.12E-05	up
Runx3	1.8	2.16E-05	4.73E-04	up
LOC100909675	1.8	1.02E-06	4.2E-05	up
A3galt2	1.8	8.12E-09	7.27E-07	up
Slfn13	1.8	1.16E-08	9.75E-07	up
Zdhhc18	1.8	5.98E-06	1.71E-04	up
Ace	1.8	4.41E-07	2.14E-05	up
Fcrl2	1.8	1.99E-04	0.003	up
Rassf1	1.8	3.97E-09	3.91E-07	up
Oasl	1.8	1.71E-04	0.002	up
Themis2	1.8	4.90E-04	0.005	up
Phldb3	1.7	5.35E-07	2.49E-05	up
Guca2a	1.7	4.5E-14	1.48E-11	up
Gadd45g	1.7	0.001	0.011	up
Bcl2l11	1.7	9.43E-09	8.17E-07	up

RGD1311892	1.7	1.23E-04	0.002	up
Grem2	1.7	3.15E-05	6.38E-04	up
Rprm	1.7	5.54E-06	1.62E-04	up
Bbc3	1.7	1.94E-05	4.37E-04	up
Cpne8	1.7	1.76E-06	6.63E-05	up
Tes	1.7	9.86E-08	5.9E-06	up
Vmp1	1.7	2.08E-08	1.61E-06	up
Lamb3	1.7	3.37E-05	6.69E-04	up
Slc16a5	1.7	6.78E-05	0.001	up
Anxa2	1.7	6.26E-09	5.8E-07	up
Gch1	1.7	0.007	0.033	up
Tns4	1.7	3.24E-04	0.004	up
Ppp2r3b	1.7	2.58E-05	5.42E-04	up
Cks2	1.7	5.81E-04	0.006	up
Enc1	1.7	2.83E-06	9.78E-05	up
Elmsan1	1.7	7.97E-10	8.96E-08	up
Il17rb	1.7	1.44E-07	8.16E-06	up
Hmga1	1.7	6.32E-05	0.001	up
Cited4	1.7	5.69E-04	0.006	up
Dusp10	1.7	0.001	0.010	up
Fam227a	1.7	4.50E-04	0.005	up
LOC100362783	1.7	0.001	0.009	up
Ifrd1	1.7	4.54E-07	2.18E-05	up
Map6	1.7	3.19E-06	1.06E-04	up
Etnk2	1.7	3.18E-05	6.40E-04	up
Gmnn	1.7	1.03E-05	2.68E-04	up
Ccnl1	1.7	1.78E-06	6.65E-05	up
Btg1	1.7	9.39E-09	8.17E-07	up
Pfkfb3	1.7	1.36E-10	1.78E-08	up
RGD1311946	1.6	2.44E-08	1.85E-06	up
Lcat	1.6	0.002	0.012	up
Fam110c	1.6	2.12E-06	7.72E-05	up
Pstpip1	1.6	1.05E-06	4.31E-05	up
Tuba1c	1.6	2.49E-05	0.000528	up
Hspb1	1.6	8.03E-05	0.001	up
B4galt5	1.6	2.51E-05	5.31E-04	up
Tfpi2	1.6	0.002	0.012	up
Rhbdf2	1.6	3.03E-06	1.02E-04	up
Sgk1	1.6	3.68E-06	1.19E-04	up
Slc2a1	1.6	8.82E-05	0.001	up
Agfg2	1.6	3.47E-08	2.45E-06	up
C1qb	1.6	5.71E-08	3.7E-06	up
Errfi1	1.6	4.98E-07	2.34E-05	up
Plk2	1.6	3.04E-08	2.23E-06	up
Efna1	1.6	4.49E-05	0.000837	up
Ier3	1.6	5.9E-11	8.64E-09	up
LOC302022	1.6	0.003	0.018	up
Snx20	1.6	6.31E-06	1.80E-04	up
Ager	1.6	0.008	0.037	up
Eno2	1.6	4.54E-04	0.005	up
Kcnk1	1.6	7.14E-07	3.12E-05	up
B3galnt1	1.6	7.46E-05	0.001	up
S100a11	1.6	7.12E-09	6.48E-07	up

Hk2	1.6	3.24E-07	1.62E-05	up
Plekhn1	1.6	0.002	0.013	up
Ren	1.6	0.003	0.017	up
Cd300a	1.5	2.61E-04	0.003	up
Pla2g2a	1.5	0.002	0.012	up
Sdc4	1.5	8.67E-06	2.34E-04	up
Cnnm4	1.5	1.67E-07	9.32E-06	up
Art4	1.5	0.007	0.035	up
LOC498276	1.5	7.41E-06	2.04E-04	up
Kcnk5	1.5	5.98E-06	1.71E-04	up
Slc25a25	1.5	1.71E-31	6.16E-28	up
Cxcl14	1.5	2.56E-04	0.003	up
Lama5	1.5	2.13E-05	4.70E-04	up
Ddit3	1.5	6.17E-05	0.001	up
Slc1a5	1.5	5.93E-06	1.71E-04	up
Tubb2b	1.5	8.32E-07	3.48E-05	up
Ppl	1.5	1.98E-11	3.35E-09	up
Ddit4	1.5	1.03E-09	1.14E-07	up
Zyx	1.5	7.54E-07	3.24E-05	up
Cd276	1.5	8.45E-06	2.29E-04	up
Ch25h	1.5	2.8E-06	9.73E-05	up
Ambp	1.5	0.004	0.025	up
Tsc22d4	1.5	9.62E-07	3.99E-05	up
Prcp	1.5	0.002	0.012	up
Jund	1.5	2.2E-10	2.77E-08	up
Csdc2	1.5	0.002	0.016	up
Pik3r5	1.5	3.60E-04	0.004	up
Wfikkn1	1.5	6.62E-04	0.006	up
Tagln	1.5	5.87E-05	0.001	up
Zfand2a	1.5	9.48E-06	2.52E-04	up
Rgs2	1.5	2.07E-09	2.17E-07	up
Zbtb16	1.5	3.67E-08	2.5E-06	up
Pkp1	1.5	2.79E-04	0.003	up
Ccl19	1.5	1.95E-04	0.003	up
C4a	1.5	4.34E-11	6.81E-09	up
Cnksr3	1.5	7.1E-07	3.11E-05	up
Pde10a	1.5	0.002	0.016	up
Gja1	1.5	5.72E-09	5.43E-07	up
Clec9a	1.5	0.003	0.021	up
RGD1305464	1.5	8.23E-07	3.47E-05	up
Lum	1.5	0.011	0.0480	up
Zbtb42	1.5	1.14E-06	4.6E-05	up
Aen	1.5	9.44E-05	0.001	up
Hspb7	1.5	5.60E-04	0.006	up
Adcy1	-1.5	8.59E-04	0.008	Down
Paqr7	-1.5	3.34E-06	1.10E-04	Down
A4galt	-1.5	2.67E-06	9.35E-05	Down
Slco1a1	-1.5	3.29E-06	1.09E-04	Down
Wscd1	-1.5	0.004	0.021	Down
Dleu7	-1.5	3.46E-08	2.45E-06	Down
Esm1	-1.6	3.18E-05	6.40E-04	Down
Hykk	-1.6	0.009	0.043	Down
RT1-T24-3	-1.7	0.002	0.016	Down

Cml1	-1.7	1.54E-06	5.89E-05	Down
RGD1559600	-1.7	0.004	0.024	Down
Pipox	-1.7	5.62E-05	9.84E-04	Down
Pdxp	-1.8	4.38E-08	2.93E-06	Down
Glyatl1	-1.8	5.74E-05	0.001	Down
Ihh	-1.8	1.43E-05	3.46E-04	Down
Sv2b	-1.8	9.67E-4	0.008	Down
Snca	-1.9	0.007	0.036	Down
Zfp93	-1.9	8.63E-04	0.008	Down
Tmem125	-1.9	0.001	0.009	Down
LOC367975	-2.0	9.24E-04	0.008	Down
Rfx6	-2.0	4.31E-05	8.14E-04	Down
Sema5b	-2.0	0.001	0.009	Down
Mylk3	-2.0	0.004	0.024	Down
Gpr63	-2.2	6.98E-05	0.001	Down
Slc16a14	-2.2	4.30E-04	0.005	Down
LOC690918	-2.2	0.001	0.010	Down
Spata22	-2.4	9.65E-12	1.74E-09	Down
Prima1	-2.4	3.33E-04	0.004	Down
Ptprq	-2.5	7.86E-06	2.15E-04	Down
Pcdh9	-2.5	0.010	0.045	Down
Ros1	-2.6	8.26E-08	5.05E-06	Down
Fam184b	-2.6	7.18E-07	3.12E-05	Down
Cyp8b1	-2.7	6.7E-05	0.001	Down
Cyp2c11l	-3.9	2.16E-18	2.13E-15	Down
Hrasls	-4.0	0.010	0.046	Down

Supplemental Table 5. IPA Enriched Canonical Pathways Between CHF+Vehicle and Sham

Ingenuity Canonical Pathway	-log(B-H *P* value)	Ratio	*z*-score	Molecules
Acute Phase Response Signaling	7.51	0.118	2.828	A2M,AMBP,C4A/C4B,CEBPB,FGA,FGB,FGG,HMOX1,IL1RN,IL6,IL6R,JUN,NFKBIA,OSMR,SERPINA3,SERPINE1,SOCS1,SOCS3,TNFRSF1A,TNFRSF1B
IL-6 Signaling	6.06	0.121	2.84	A2M,CD14,CEBPB,HSPB1,HSPB7,IL1R2,IL1RN,IL6,IL6R,JUN,NFKBIA,PIK3R5,SOCS1,SOCS3,TNFRSF1A,TNFRSF1B
Granulocyte Adhesion and Diapedesis	5.96	0.108	Not predicted	CCL19,CLDN4,CLDN7,CSF3,CXCL10,CXCL14,CXCL2,CXCL3,CXCR4,HSPB1,IL1R2,IL1RN,ITGB3,SDC4,SELP,TNFRSF1A,TNFRSF1B
Osteoarthritis Pathway	5.81	0.092	1	ADAMTS4,AGER,ANXA2,CEBPB,CREB5,DDIT4,ELF3,IHH,IL1R2,PRG4,PTHLH,S100A8,S100A9,SDC4,SOX9,SPHK1,SPP1,TNFRSF1A,TNFRSF1B
LXR/RXR Activation	5.71	0.126	0	AMBP,C4A/C4B,CD14,CLU,FGA,IL1R2,IL1RN,IL6,LCAT,LDLR,S100A8,TNFRSF1A,TNFRSF1B,UGT1A3
p38 MAPK Signaling	4.72	0.113	2.496	CREB5,DDIT3,DUSP1,DUSP10,HSPB1,HSPB7,IL1R2,IL1RN,MYC,PLA2G2A,TIFA,TNFRSF1A,TNFRSF1B
IL-10 Signaling	4.54	0.149	Not predicted	CD14,FCGR2A,FCGR2B,HMOX1,IL1R2,IL1RN,IL6,JUN,NFKBIA,SOCS3
IL-17A Signaling in Fibroblasts	3.94	0.212	Not predicted	CEBPB,CEBPD,IL6,JUN,LCN2,NFKBIA,NFKBIZ
Coagulation System	3.80	0.200	0.378	A2M,BDKRB2,FGA,FGB,FGG,PLAUR,SERPINE1
Hepatic Fibrosis / Hepatic Stellate Cell Activation	3.41	0.077	Not predicted	A2M,CCN2,CD14,COL7A1,CXCL3,EDN1,IL1R2,IL6,IL6R,KLF6,SERPINE1,TIMP1,TNFRSF1A,TNFRSF1B
VDR/RXR Activation	3.22	0.115	0.816	CD14,CDKN1A,CEBPB,CXCL10,GADD45A,IGFBP1,KLF4,SPP1,TRPV6
Agranulocyte Adhesion and Diapedesis	3.20	0.078	Not predicted	CCL19,CLDN4,CLDN7,CXCL10,CXCL14,CXCL2,CXCL3,CXCR4,Glycam1,IL1RN,SDC4,SELP,TNFRSF1A
Role of Tissue Factor in Cancer	3.02	0.087	Not predicted	CCN1,CCN2,F2RL1,FGA,FGB,FGG,HBEGF,ITGB3,PDXP,PIK3R5,PLAUR
Role of	3.01	0.0	Not	ADAMTS4,CEBPB,CEBPD,CREB5,F2RL1,IL1R2,IL1RN,IL6,IL6R,IL7,JUN,MYC,NFKBIA,PIK3R5,SOCS1,S

Macrophages, Fibroblasts and Endothelial Cells in Rheumatoid Arthritis		57	predicted	OCS3,TNFRSF1A,TNFRSF1B
Atherosclerosis Signaling	2.65	0.085	Not predicted	ALOX15,CLU,CXCR4,IL1RN,IL6,LCAT,PLA2G2A,S100A8,SELP,TNFRSF12A
Role of JAK family kinases in IL-6-type Cytokine Signaling	2.64	0.200	Not predicted	IL6,IL6R,OSMR,SOCS1,SOCS3
Th1 and Th2 Activation Pathway	2.62	0.071	Not predicted	CXCR4,IL17RB,IL24,IL6,IL6R,IRF1,JUN,NFIL3,PIK3R5,RUNX3,SOCS1,SOCS3
Glucocorticoid Receptor Signaling	2.43	0.052	Not predicted	A2M,CDKN1A,CEBPB,CXCL3,DUSP1,FGG,FKBP5,HSPA1A/HSPA1B,IL1R2,IL1RN,IL6,JUN,KRT18,NFKBIA,PIK3R5,SERPINE1,SGK1
Hepatic Cholestasis	2.43	0.071	Not predicted	ADCY1,CD14,CYP8B1,IL1R2,IL1RN,IL6,JUN,LIF,NFKBIA,TNFRSF1A,TNFRSF1B
ERK5 Signaling	2.21	0.100	2.449	CREB5,FOSL1,LIF,MAP3K8,MYC,SGK1,SH2D2A
Role of IL-17A in Psoriasis	2.21	0.375	Not predicted	CXCL3,S100A8,S100A9
D-myo-inositol (1,4,5,6)-Tetrakisphosphate Biosynthesis	2.21	0.071	2.53	CA3,DUSP1,DUSP10,DUSP2,DUSP5,DUSP8,MINPP1,PDXP,Ppp2r3d,SOCS3
D-myo-inositol (3,4,5,6)-tetrakisphosphate	2.21	0.071	2.53	CA3,DUSP1,DUSP10,DUSP2,DUSP5,DUSP8,MINPP1,PDXP,Ppp2r3d,SOCS3

Biosynthesis				
GADD45 Signaling	2.19	0.211	Not predicted	CDKN1A,GADD45A,GADD45B,GADD45G
Role of Osteoblasts, Osteoclasts and Chondrocytes in Rheumatoid Arthritis	2.12	0.057	Not predicted	ADAMTS4,BIRC3,IL1R2,IL1RN,IL6,IL7,ITGB3,JUN,NFKBIA,PIK3R5,SPP1,TNFRSF1A,TNFRSF1B
Role of Cytokines in Mediating Communication between Immune Cells	1.98	0.132	Not predicted	CSF3,IL1RN,IL23A,IL24,IL6
3-phosphoinositide Degradation	1.98	0.065	2.53	CA3,DUSP1,DUSP10,DUSP2,DUSP5,DUSP8,MINPP1,PDXP,Ppp2r3d,SOCS3
Apelin Cardiac Fibroblast Signaling Pathway	1.98	0.182	-2	CCN2,IL6,SERPINE1,SPHK1
IL-12 Signaling and Production in Macrophages	1.97	0.069	Not predicted	ALOX15,CEBPB,CLU,IL23A,IRF1,JUN,MAP3K8,PIK3R5,S100A8
Production of Nitric Oxide and Reactive Oxygen Species in Macrophages	1.97	0.060	3.317	CLU,IRF1,JUN,MAP3K6,MAP3K8,NFKBIA,PIK3R5,RHOB,S100A8,TNFRSF1A,TNFRSF1B
Hematopoiesis from Pluripotent	1.97	0.128	Not predicted	CSF3,EPO,IL6,IL7,LIF

Stem Cells				
D-myo-inositol-5-phosphate Metabolism	1.97	0.063	2.53	CA3,DUSP1,DUSP10,DUSP2,DUSP5,DUSP8,MINPP1,PDXP,Ppp2r3d,SOCS3
GP6 Signaling Pathway	1.97	0.069	3	COL7A1,FGA,FGB,FGG,ITGB3,LAMA5,LAMB3,LAMC2,PIK3R5
p53 Signaling	1.96	0.075	0	BBC3,CDKN1A,GADD45A,GADD45B,GADD45G,JUN,PIK3R5,RPRM
Induction of Apoptosis by HIV1	1.96	0.098	0.816	BBC3,BIRC3,CXCR4,NFKBIA,TNFRSF1A,TNFRSF1B
HMGB1 Signaling	1.96	0.068	2.828	AGER,IL6,JUN,LIF,PIK3R5,RHOB,SERPINE1,TNFRSF1A,TNFRSF1B
Hematopoiesis from Multipotent Stem Cells	1.96	0.273	Not predicted	CSF3,EPO,IL7
IGF-1 Signaling	1.93	0.073	0	CCN1,CCN2,CCN3,IGFBP1,JUN,PIK3R5,SOCS1,SOCS3
Prolactin Signaling	1.86	0.080	0.816	CEBPB,IRF1,JUN,MYC,PIK3R5,SOCS1,SOCS3
iNOS Signaling	1.86	0.114	Not predicted	CD14,HMGA1,IRF1,JUN,NFKBIA
3-phosphoinositide Biosynthesis	1.86	0.056	2.714	CA3,DUSP1,DUSP10,DUSP2,DUSP5,DUSP8,MINPP1,PDXP,PIK3R5,Ppp2r3d,SOCS3
JAK/Stat Signaling	1.84	0.079	0.378	CDKN1A,CEBPB,IL6,JUN,PIK3R5,SOCS1,SOCS3
Superpathway of Inositol Phosphate Compounds	1.81	0.052	2.887	CA3,DUSP1,DUSP10,DUSP2,DUSP5,DUSP8,ITPKC,MINPP1,PDXP,PIK3R5,Ppp2r3d,SOCS3
IL-7 Signaling Pathway	1.81	0.077	0.816	BCL6,IL7,JUN,MYC,PIK3R5,SLC2A1,SOCS1
Germ Cell-Sertoli Cell Junction	1.81	0.058	Not predicted	A2M,MAP3K6,MAP3K8,PIK3R5,RHOB,TNFRSF1A,TUBA1C,TUBB2B,TUBB6,ZYX

Signaling				
Dendritic Cell Maturation	1.80	0.058	3	CREB5,FCGR2A,FCGR2B,IL1RN,IL23A,IL6,NFKBIA,PIK3R5,TNFRSF1A,TNFRSF1B
ATM Signaling	1.72	0.073	Not predicted	CDKN1A,CREB5,GADD45A,GADD45B,GADD45G,JUN,NFKBIA
TNFR2 Signaling	1.72	0.133	1	BIRC3,JUN,NFKBIA,TNFRSF1B
Sertoli Cell-Sertoli Cell Junction Signaling	1.72	0.056	Not predicted	A2M,CLDN4,CLDN7,JUN,MAP3K6,MAP3K8,TNFRSF1A,TUBA1C,TUBB2B,TUBB6
Th1 Pathway	1.70	0.065	0.707	IL6,IL6R,IRF1,NFIL3,PIK3R5,RUNX3,SOCS1,SOCS3
Glioma Invasiveness Signaling	1.64	0.080	1.633	CD44,ITGB3,PIK3R5,PLAUR,RHOB,TIMP1
Role of JAK2 in Hormone-like Cytokine Signaling	1.64	0.125	Not predicted	EPO,SH2B2,SOCS1,SOCS3
Extrinsic Prothrombin Activation Pathway	1.63	0.188	Not predicted	FGA,FGB,FGG
Adipogenesis pathway	1.58	0.061	Not predicted	ARNTL,CEBPB,CEBPD,DDIT3,EGR2,KLF5,SOX9,TNFRSF1A
Neuroinflammation Signaling Pathway	1.54	0.045	2.887	AGER,BIRC3,CREB5,CXCL10,HMOX1,IL6,IL6R,JUN,PIK3R5,PLA2G2A,S100B,SNCA,TNFRSF1A
NRF2-mediated Oxidative Stress Response	1.53	0.051	1.89	ENC1,FKBP5,FOSL1,GPX2,HMOX1,JUN,JUNB,JUND,MAFF,PIK3R5
Complement System	1.53	0.114	1	C1QB,C4A/C4B,CFD,CFI

The significance values (*P* value of overlap) for the canonical pathways are calculated by the right-tailed Fisher's Exact Test. The ratio is the number of molecules in a given pathway divided by the total number of molecules that make up that pathway and that are in the reference set. *Z*-scores indicate activity of a pathway. Positive *z*-scores indicate activation,and negative *z*-score predicts overall decrease in activity.

Supplemental Table 6. Differentially Expressed Genes Between CHF+Veh and CHF+RTX

Gene	log2 Fold Change	*P* value	*P* adj	Direction
Cyp2c11l	3.5	2.05E-12	3.17E-09	up
Serpinb12	3.5	0.003	0.041	up
Mchr1	3.0	5.88E-05	0.003	up
Scd1	2.6	4.62E-04	0.012	up
Ptprq	2.5	5.17E-05	0.003	up
Sds	2.4	3.42E-04	0.010	up
Ros1	2.3	3.03E-05	0.002	up
Armc3	2.2	0.002	0.029	up
Fzd5	2.0	1.47E-14	5.30E-11	up
Anxa13	2.0	7.66E-05	0.003	up
Arl5b	1.9	1.99E-12	3.17E-09	up
Cabp7	1.8	0.003	0.037	up
Slco1a1	1.8	6.12E-07	8.95E-05	up
Coq10b	1.7	5.80E-08	1.21E-05	up
Ccdc114	1.7	2.91E-04	0.008695	up
Fbxo32	1.7	1.73E-08	4.56E-06	up
Phf21b	1.7	0.003	0.041	up
Yod1	1.7	2.98E-10	1.50E-07	up
Gramd1b	1.6	2.14E-08	5.53E-06	up
Upp2	1.6	1.14E-08	3.26E-06	up
Pou3f1	1.6	6.28E-04	0.014	up
Spata22	1.6	4.07E-05	0.002	up
Slc1a4	1.6	2.33E-06	2.47E-04	up
Gnat1	1.5	2.86E-04	0.009	up
Irf4	1.5	5.89E-04	0.014	up
Egfr	1.5	2.81E-05	0.002	up
Ddx25	1.5	3.46E-04	0.010	up
Prdm1	1.5	1.38E-04	0.005	up
Rcsd1	-1.5	0.003	0.035	down
Gja5	-1.5	4.86E-05	0.002	down
Apoc2	-1.5	0.003	0.038	down
Sash3	-1.5	0.003	0.037	down
Tgfb2	-1.5	2.06E-04	0.007	down
Tlr4	-1.5	0.002	0.035	down
Ccnb2	-1.5	0.001	0.020	down
Prtfdc1	-1.5	0.002	0.033	down
Marcks	-1.5	7.91E-09	2.48E-06	down
Olfml3	-1.5	1.23E-04	0.005	down
Dlgap5	-1.5	7.68E-04	0.016	down
Cmtm3	-1.5	6.43E-05	0.003	down
Lyz2	-1.5	1.14E-18	1.23E-14	down
Chst12	-1.5	3.01E-04	0.009	down
Dcn	-1.5	3.04E-10	1.50E-07	down
Cyp26b1	-1.5	0.003	0.037	down
Selplg	-1.6	0.002	0.028	down
Traf1	-1.6	0.004	0.050	down
Bst1	-1.6	2.79E-04	0.008	down
Cd44	-1.6	1.93E-05	0.001	down
Ect2	-1.6	2.02E-04	0.007	down
Tnfsf10	-1.6	5.35E-05	0.003	down
Top2a	-1.6	9.25E-06	7.15E-04	down

Spi1	-1.6	2.27E-05	0.001	down
Baat	-1.6	8.61E-04	0.018	down
Cd200	-1.6	1.83E-04	0.006	down
Znrd1as1	-1.6	5.89E-05	0.003	down
Pou2af1	-1.6	0.004	0.048	down
Tbxas1	-1.6	2.71E-06	2.77E-04	down
Gngt2	-1.6	6.99E-06	5.82E-04	down
Dkk3	-1.6	3.49E-04	0.010	down
Fcrl2	-1.6	0.002	0.034	down
Ccl21	-1.6	3.74E-05	0.002	down
Adamts2	-1.7	0.003	0.042	down
Axl	-1.7	1.66E-05	0.001	down
Hfe2	-1.7	0.003	0.036	down
Adgre1	-1.7	4.74E-05	0.002	down
Hmx2	-1.7	0.000227	0.007	down
Plek	-1.7	1.01E-07	1.88E-05	down
C6	-1.7	0.002	0.031	down
Nov	-1.8	0.003	0.041	down
Pycard	-1.8	7.21E-06	5.96E-04	down
Mki67	-1.8	1.00E-09	4.01E-07	down
Egflam	-1.8	4.92E-04	0.012	down
Hacd4	-1.8	0.002	0.034	down
Lgals1	-1.8	8.83E-11	7.63E-08	down
Alox15	-1.8	3.19E-05	0.002	down
Pnma2	-1.8	0.003	0.038	down
Emp3	-1.8	3.17E-06	3.10E-04	down
Scara3	-1.8	5.01E-05	0.003	down
Rab3il1	-1.8	5.89E-04	0.014	down
Srpx2	-1.8	1.49E-04	0.006	down
Lck	-1.8	3.50E-05	0.002	down
Rem1	-1.8	6.25E-05	0.003	down
B3galt2	-1.9	6.23E-04	0.014	down
Sox18	-1.9	0.002	0.034	down
Igsf6	-1.9	2.55E-05	0.002	down
Tlr8	-2.0	4.11E-04	0.011	down
Clec12a	-2.0	2.57E-06	2.70E-04	down
Loxl1	-2.0	1.90E-10	1.21E-07	down
Clec4a1	-2.0	5.46E-05	0.003	down
Cfi	-2.0	5.68E-08	1.21E-05	down
Evi2a	-2.0	0.002	0.027	down
Ccl19	-2.1	9.16E-06	7.15E-04	down
Tril	-2.1	6.56E-04	0.015	down
Arl11	-2.1	1.06E-06	1.33E-04	down
Trpc6	-2.1	8.98E-04	0.018	down
Eln	-2.1	8.01E-05	0.003	down
Agtr1b	-2.2	1.92E-04	0.006	down
Srms	-2.2	0.004	0.049	down
Gpr34	-2.2	0.001	0.021	down
Ptprz1	-2.2	4.25E-04	0.011	down
Upk3bl	-2.2	7.83E-05	0.003	down
Lum	-2.2	0.001	0.025	down
Cenpf	-2.2	6.03E-07	8.95E-05	down
C5ar1	-2.2	2.22E-04	0.007	down

LOC100365008	-2.2	0.002	0.026	down
Hsd17b2	-2.3	3.01E-04	0.009	down
Adra1d	-2.3	0.001	0.020	down
Folr2	-2.3	3.33E-04	0.009	down
Fibin	-2.4	4.02E-05	0.002	down
Col1a1	-2.4	8.03E-09	2.48E-06	down
C4b	-2.4	9.30E-13	2.01E-09	down
Clec4a3	-2.4	1.16E-09	4.50E-07	down
Il20ra	-2.5	0.004	0.049	down
Lilra5	-2.5	0.003	0.037	down
Gpnmb	-2.7	2.62E-06	2.73E-04	down
Kng1l1	-2.7	1.73E-04	0.006	down
Fam180a	-2.9	4.76E-06	4.26E-04	down
Cxcl13	-3.1	1.58E-04	0.006	down
Scara5	-3.1	2.12E-04	0.007	down
Cyp3a9	-3.2	8.56E-04	0.018	down
Havcr1	-4.4	4.60E-06	4.19E-04	down
Ubd	-4.5	2.14E-04	0.007	down
Il24	-6.0	2.78E-04	0.008	down
Fam111a	-7.7	2.15E-05	0.001	down

Supplemental Table 7. IPA Enriched Canonical Pathways Between CHF+Vehicle and CHF+RTX

Ingenuity Canonical Pathway	-log(*P* value)	Ratio	*z*-score	Molecules
IL-12 Signaling and Production in Macrophages	3.85	0.046	Not predicted	ALOX15,APOC2,LYZ,SPI1,TGFB2,TLR4
LXR/RXR Activation	3.24	0.045	0	APOC2,C4A/C4B,LYZ,SCD,TLR4
Wnt/β-catenin Signaling	3.24	0.036	1.342	CD44,DKK3,FZD5,SOX18,TGFB2,UBD
Atherosclerosis Signaling	3.12	0.042	Not predicted	ALOX15,APOC2,COL1A1,LYZ,SELPLG
Hepatic Fibrosis / Hepatic Stellate Cell Activation	3.08	0.033	Not predicted	Agtr1b,CCL21,COL1A1,EGFR,TGFB2,TLR4
Phagosome Formation	3.02	0.040	Not predicted	C5AR1,Fcrls,SCARA3,TLR4,TLR8
Toll-like Receptor Signaling	2.97	0.054	Not predicted	TLR4,TLR8,TRAF1,UBD
Complement System	2.91	0.086	Not predicted	C4A/C4B,C5AR1,CFI
Altered T Cell and B Cell Signaling in Rheumatoid Arthritis	2.75	0.047	Not predicted	CCL21,CXCL13,TLR4,TLR8
Granulocyte Adhesion and Diapedesis	2.57	0.032	Not predicted	C5AR1,CCL19,CCL21,CXCL13,SELPLG
Agranulocyte Adhesion and Diapedesis	2.45	0.030	Not predicted	C5AR1,CCL19,CCL21,CXCL13,SELPLG
Inflammasome pathway	2.24	0.105	Not predicted	PYCARD,TLR4
Role of Pattern Recognition Receptors in Recognition of Bacteria and Viruses	2.09	0.031	Not predicted	C5AR1,TGFB2,TLR4,TLR8
Role of Macrophages, Fibroblasts and Endothelial Cells in Rheumatoid Arthritis	1.91	0.019	Not predicted	C5AR1,DKK3,FZD5,TLR4,TLR8,TRAF1
L-serine Degradation	1.74	0.333	Not predicted	SDS
Colorectal Cancer Metastasis Signaling	1.74	0.020	0	EGFR,FZD5,TGFB2,TLR4,TLR8
Tec Kinase Signaling	1.73	0.024	Not predicted	GNAT1,LCK,TLR4,TNFSF10
Estrogen Biosynthesis	1.61	0.050	Not predicted	CYP3A7,HSD17B2
NF-κB Signaling	1.60	0.022	-1	EGFR,LCK,TLR4,TLR8
Production of Nitric Oxide and Reactive Oxygen Species in Macrophages	1.58	0.022	Not predicted	APOC2,LYZ,SPI1,TLR4
Neuroinflammation Signaling Pathway	1.49	0.017	-1.342	CD200,PYCARD,TGFB2,TLR4,TLR8
FXR/RXR Activation	1.46	0.026	Not predicted	APOC2,BAAT,C4A/C4B
Cell Cycle: G2/M DNA Damage Checkpoint Regulation	1.43	0.040	Not predicted	CCNB2,TOP2A

Phototransduction Pathway	1.43	0.040	Not predicted	GNAT1,GNGT2
LPS/IL-1 Mediated Inhibition of RXR Function	1.40	0.019	Not predicted	APOC2,CHST12,CYP3A7,TLR4

The significance values (*P* value of overlap) for the canonical pathways are calculated by the right-tailed Fisher's Exact Test. The ratio is the number of molecules in a given pathway divided by the total number of molecules that make up that pathway and that are in the reference set. Z-scores indicate activity of a pathway. Positive *z*-scores indicate activation, and negative z-score predicts overall decrease in activity.